Probing the anomalous triple gauge boson couplings in $e^+e^- \to W^+W^-$ using W polarizations with polarized beams

Rafiqul Rahaman[*] and Ritesh K. Singh[†]

Department of Physical Sciences, Indian Institute of Science Education and Research Kolkata, Mohanpur 741246, India

(Received 15 November 2019; accepted 21 March 2020; published 24 April 2020)

We study the anomalous W^+W^-V ($V = \gamma, Z$) couplings in $e^+e^- \to W^+W^-$ using the complete set of polarization observables of W boson with longitudinally polarized electron (e^-) and positron (e^+) beams. For the effective W^+W^-V couplings, we use the most general Lorentz invariant form factor parametrization as well as $SU(2) \times U(1)$ invariant dimension-6 effective operators. We estimate simultaneous limits on the anomalous couplings using the Markov-chain Monte Carlo method for an e^+e^- collider running at the center of mass energy of $\sqrt{s} = 500$ GeV and the integrated luminosity of $\mathcal{L} = 100$ fb^{-1}, 3.2 ab^{-1} and 4 ab^{-1}. The best limits on the anomalous couplings are obtained for e^- and e^+ polarization being $(\pm 0.8, \mp 0.6)$ for both 100 fb^{-1} and 3.2 ab^{-1} of luminosity.

DOI: 10.1103/PhysRevD.101.075044

I. INTRODUCTION

The non-Abelian gauge symmetry $SU(2) \times U(1)$ of the Standard Model (SM) allows the WWV ($V = \gamma,\ Z$) couplings after the electroweak symmetry breaking (EWSB) by the Higgs field discovered at the large hadron collider (LHC) [1]. To test the EWSB, the WWV couplings have to be measured precisely, which is still lacking. We intend to study the measurement of these couplings using polarization observables of the spin-1 boson [2–8]. To test the SM WWV couplings, one has to hypothesize beyond the SM (BSM) couplings and make sure they do not appear at all or are severely constrained. One approach is to consider $SU(2) \times U(1)$ invariant higher dimension effective operators which provide the WWV form factors after EWSB [9]. The effective Lagrangian considering the higher dimension operators can be written as

$$\mathcal{L}_{eft} = \mathcal{L}_{\rm SM} + \sum_i \frac{c_i^{\mathcal{O}(6)}}{\Lambda^2}\mathcal{O}_i^{(6)} + \sum_i \frac{c_i^{\mathcal{O}(8)}}{\Lambda^4}\mathcal{O}_i^{(8)} + \cdots, \quad (1)$$

where $c_i^{\mathcal{O}(6,8)}$ are the couplings of the higher dimension operators $\mathcal{O}_i^{(6,8)}$ and Λ is the energy scale below which the theory is valid. To the lowest order (up to dimension-6) the operators contributing to WWV couplings are [10,11]

$$\begin{aligned}
\mathcal{O}_{WWW} &= \mathrm{Tr}[W_{\mu\nu}W^{\nu\rho}W^{\mu}_{\rho}],\\
\mathcal{O}_W &= (D_\mu\Phi)^\dagger W^{\mu\nu}(D_\nu\Phi),\\
\mathcal{O}_B &= (D_\mu\Phi)^\dagger B^{\mu\nu}(D_\nu\Phi),\\
\mathcal{O}_{\widetilde{WWW}} &= \mathrm{Tr}[\tilde{W}_{\mu\nu}W^{\nu\rho}W^{\mu}_{\rho}],\\
\mathcal{O}_{\tilde{W}} &= (D_\mu\Phi)^\dagger \tilde{W}^{\mu\nu}(D_\nu\Phi),
\end{aligned} \quad (2)$$

where Φ is the Higgs doublet field and

$$\begin{aligned}
D_\mu &= \partial_\mu + \frac{i}{2}g\tau^I W^I_\mu + \frac{i}{2}g' B_\mu,\\
W_{\mu\nu} &= \frac{i}{2}g\tau^I(\partial_\mu W^I_\nu - \partial_\nu W^I_\mu + g\varepsilon_{IJK}W^J_\mu W^K_\nu),\\
B_{\mu\nu} &= \frac{i}{2}g'(\partial_\mu B_\nu - \partial_\nu B_\mu).
\end{aligned} \quad (3)$$

Here g and g' are the $SU(2)$ and $U(1)$ couplings, respectively. Among these operators, $\mathcal{O}_{WWW}$, $\mathcal{O}_W$, and $\mathcal{O}_B$ are CP even, while $\mathcal{O}_{\widetilde{WWW}}$ and $\mathcal{O}_{\tilde{W}}$ are CP odd. These effective operators, after EWSB, also provide HZV and HWW couplings, which can be examined in various processes, e.g., $ZV/ZW/HV/HW$ production processes. These processes may contain some other effective operators as well. We note that the W pair production process also contains anomalous couplings other than the aTGC [12,13]. However, for simplicity, we study this process only with the anomalous gauge boson couplings.

[*] rr13rs033@iiserkol.ac.in
[†] ritesh.singh@iiserkol.ac.in

The other alternative to step beyond the SM WWV structure is to consider the most general Lorentz invariant effective form factors in a model independent way. A Lagrangian for the above parametrization is given by [14]

$$\begin{aligned}\mathcal{L}_{WWV} = & ig_{WWV}(g_1^V(W^+_{\mu\nu}W^{-\mu} - W^{+\mu}W^-_{\mu\nu})V^\nu \\ & + ig_4^V W^+_\mu W^-_\nu(\partial^\mu V^\nu + \partial^\nu V^\mu) \\ & - ig_5^V \varepsilon^{\mu\nu\rho\sigma}(W^+_\mu \partial_\rho W^-_\nu - \partial_\rho W^+_\mu W^-_\nu)V_\sigma \\ & + \frac{\lambda^V}{m_W^2} W^{+\nu}_\mu W^{-\rho}_\nu V^\mu_\rho + \frac{\widetilde{\lambda^V}}{m_W^2} W^{+\nu}_\mu W^{-\rho}_\nu \tilde{V}^\mu_\rho \\ & + \kappa^V W^+_\mu W^-_\nu V^{\mu\nu} + \widetilde{\kappa^V} W^+_\mu W^-_\nu \tilde{V}^{\mu\nu}). \end{aligned} \tag{4}$$

Here $W^\pm_{\mu\nu} = \partial_\mu W^\pm_\nu - \partial_\nu W^\pm_\mu$, $V_{\mu\nu} = \partial_\mu V_\nu - \partial_\nu V_\mu$, $\tilde{V}^{\mu\nu} = 1/2\varepsilon^{\mu\nu\rho\sigma}V_{\rho\sigma}$, and the overall coupling constants are defined as $g_{WW\gamma} = -g\sin\theta_W$ and $g_{WWZ} = -g\cos\theta_W$, with θ_W being the weak mixing angle. In the SM, $g_1^V = 1$, $\kappa^V = 1$ and other couplings are zero. The anomalous part in g_1^V, κ^V would be $\Delta g_1^V = g_1^V - 1$, $\Delta\kappa^V = \kappa^V - 1$, respectively. The couplings g_1^V, κ^V and λ^V are CP even (both C and P even), while g_4^V (odd in C, even in P), $\widetilde{\kappa^V}$ and $\widetilde{\lambda^V}$ (even in C, odd in P) are CP odd. On the other hand g_5^V is both C and P odd making it CP even. We label these sets of 14 anomalous couplings to be $c_i^{\mathcal{L}}$ as given in Eq. (A2) in Appendix A for later uses.

On restricting to the $SU(2) \times U(1)$ gauge, the coupling $(c_i^{\mathcal{L}})$ of the Lagrangian in Eq. (4) can be written in terms of the couplings of the operators in Eq. (2) as [10,11,14,15]

$$\begin{aligned} \Delta g_1^Z &= c_W \frac{m_Z^2}{2\Lambda^2}, \\ g_4^V &= g_5^V = \Delta g_1^\gamma = 0, \\ \lambda^\gamma &= \lambda^Z = \lambda^V = c_{WWW}\frac{3g^2m_W^2}{2\Lambda^2}, \\ \widetilde{\lambda^\gamma} &= \widetilde{\lambda^Z} = \widetilde{\lambda^V} = c_{\widetilde{WWW}}\frac{3g^2m_W^2}{2\Lambda^2}, \\ \Delta\kappa^\gamma &= (c_W + c_B)\frac{m_W^2}{2\Lambda^2}, \\ \Delta\kappa^Z &= (c_W - c_B\tan^2\theta_W)\frac{m_W^2}{2\Lambda^2}, \\ \widetilde{\kappa^\gamma} &= c_{\widetilde{W}}\frac{m_W^2}{2\Lambda^2}, \\ \widetilde{\kappa^Z} &= -c_{\widetilde{W}}\tan^2\theta_W\frac{m_W^2}{2\Lambda^2}. \end{aligned} \tag{5}$$

It is clear from above that some of the vertex factor couplings are dependent on each other and they are

$$\begin{aligned} \Delta g_1^Z &= \Delta\kappa^Z + \tan^2\theta_W\Delta\kappa^\gamma, \\ \widetilde{\kappa^Z} &+ \tan^2\theta_W\widetilde{\kappa^\gamma} = 0. \end{aligned} \tag{6}$$

We label the nonvanishing nine couplings in $SU(2) \times U(1)$ gauge as $c_i^{\mathcal{L}_g}$ given in Eq. (A2) in Appendix A for later uses.

The anomalous WWV couplings have been studied in the effective operator approach as well as in the effective vertex formalism subjected to $SU(2) \times U(1)$ invariance for the $e^+ - e^-$ collider [12,14,16–25], Large Hadron electron collider (LHeC) [26–28], e-γ collider [29], and LHC [13,24,25,30–41]. Some CP-odd WWV couplings have been studied in Refs. [20,36,40].

On the experimental side, the anomalous WWV couplings have been explored and stringent limits on them have been obtained at the LEP [3,42–44], the Tevatron [45,46], the LHC [47–62], and Tevatron-LHC [63]. The tightest one parameter limit obtained on the anomalous couplings from experiments are given in Table I. The tightest limits on operator couplings $(c_i^{\mathcal{O}})$ are obtained in Ref. [60] for CP-even ones and in Ref. [58] for CP-odd ones. These limits translated to $c_i^{\mathcal{L}_g}$ using Eq. (5) are also given in Table I. The tightest limits on the couplings g_4^Z and g_5^Z are obtained in Refs. [42,43] considering the Lagrangian in Eq. (4).

The W^+W^- production is one of the important processes to be studied at the future International Linear Collider (ILC) [64–66] for the precision test [67] as well as for BSM physics. This process has been studied earlier for SM phenomenology as well as for various BSM physics with and without beam polarization [14,68–72]. Here we intend to study WWV anomalous couplings in $e^+e^- \to W^+W^-$ at $\sqrt{s} = 500$ GeV and integrated luminosity of $\mathcal{L} = 100$ fb^{-1} using the cross section, forward-backward asymmetry, and eight polarizations asymmetries of W^- for a set of choices of longitudinally polarized e^+ and e^- beams in the channel $W^- \to l^-\bar{\nu}_l$ $(l = e,\ \mu)$[1] and $W^+ \to$ hadrons. The polarizations of Z and W are being used widely recently for various BSM studies [73–79] along with studies with anomalous gauge boson couplings [3,7,80,81]. Recently, the polarizations of W/Z have been measured in WZ production at the LHC [82]. Besides the final state polarizations, the initial state beam polarizations at the ILC can be used to enhance the relevant signal to background ratio [67,70,72,83,84]. It also has the ability to distinguish between CP-even and CP-odd couplings [67,85–94]. We note that an e^+e^- machine will run with longitudinal beam polarizations switching between (η_3, ξ_3) and $(-\eta_3, -\xi_3)$ [67], where $\eta_3(\xi_3)$ is the longitudinal polarization of e^- (e^+). For an integrated luminosity of 100 fb^{-1}, one will

[1]For simplicity we do not include the tau decay mode as the tau decays to the neutrino within the beam pipe, giving extra missing momenta affecting the reconstruction of the events.

TABLE I. The list of tightest limits obtained on the anomalous couplings of dimension-6 operators in Eq. (2) and effective vertices in Eq. (4) in the $SU(2) \times U(1)$ gauge (except g_4^Z and g_5^Z) at 95% C.L. from experiments.

$c_i^{\mathcal{O}}$	Limits (TeV^{-2})	Remark
$\frac{c_{WWW}}{\Lambda^2}$	$[-1.58, +1.59]$	CMS $\sqrt{s} = 13$ TeV, $\mathcal{L} = 35.9$ fb^{-1}, $SU(2) \times U(1)$ [60]
$\frac{c_W}{\Lambda^2}$	$[-2.00, +2.65]$	CMS [60]
$\frac{c_B}{\Lambda^2}$	$[-8.78, +8.54]$	CMS [60]
$\frac{c_{\widetilde{WWW}}}{\Lambda^2}$	$[-11, +11]$	ATLAS $\sqrt{s} = 7(8)$ TeV, $\mathcal{L} = 4.7(20.2)$ fb^{-1} [58]
$\frac{c_{\widetilde{W}}}{\Lambda^2}$	$[-580, 580]$	ATLAS [58]
$c_i^{\mathcal{L}_g}$	Limits ($\times 10^{-2}$)	Remark
λ^V	$[-0.65, +0.66]$	CMS [60]
$\Delta\kappa^\gamma$	$[-4.4, +6.3]$	CMS $\sqrt{s} = 8$ TeV, $\mathcal{L} = 19$ fb^{-1}, $SU(2) \times U(1)$ [57]
Δg_1^Z	$[-0.61, +0.74]$	CMS [60]
$\Delta\kappa^Z$	$[-0.79, +0.82]$	CMS [60]
$\widetilde{\lambda^V}$	$[-4.7, +4.6]$	ATLAS [58]
$\widetilde{\kappa^Z}$	$[-14, -1]$	DELPHI (LEP2), $\sqrt{s} = 189$–209 GeV, $\mathcal{L} = 520$ pb^{-1} [43]
$c_i^{\mathcal{L}}$	Limits ($\times 10^{-2}$)	Remark
g_4^Z	$[-59, -20]$	DELPHI [43]
g_5^Z	$[-16, +9.0]$	OPAL (LEP), $\sqrt{s} = 183$–209 GeV, $\mathcal{L} = 680$ pb^{-1} [42]

have half the luminosity available for each polarization configuration. The most common observables, the cross section, for example, studied in literature with beam polarizations are the total cross section

$$\sigma_T(\eta_3, \xi_3) = \sigma(+\eta_3, +\xi_3) + \sigma(-\eta_3, -\xi_3) \tag{7}$$

and the difference

$$\sigma_A(\eta_3, \xi_3) = \sigma(+\eta_3, +\xi_3) - \sigma(-\eta_3, -\xi_3). \tag{8}$$

We find that combining the two opposite beam polarizations at the level of χ^2 rather than combining them as in Eqs. (7) and (8), we can constrain the anomalous couplings better in this analysis; see Appendix C for explanation.

We note that there exist 64 polarization correlations [14] apart from $8 + 8$ polarizations for W^+ and W^-. The measurement of these correlations requires the identification of light quark flavors in the above channel, which is not possible; hence, we are not including polarization correlations in our analysis. In the case of both the Ws decaying leptonicaly, there are two missing neutrinos and reconstruction of polarization observables suffers combinatorial ambiguity. Here we aim to work with a set of observables that can be reconstructed uniquely and test their ability to probe the anomalous couplings including partial contribution up to $\mathcal{O}(\Lambda^{-4})$.[2] The rest of the paper is arranged in the following way. In Sec. II we introduce the complete set polarization observables of a spin-1 particle along with the forward-backward asymmetry and study the effect of beam polarizations on the observables. In Sec. III we use the vertex form factors for the Lagrangian in Eq. (4) and obtain expressions for all the observables. In this section, we cross-validate analytical results against the numerical result from MadGraph5 [95] for sanity checking. We also study the $\cos\theta$ (of W) dependences of the observables and study their sensitivity on the anomalous couplings. In this section, we also estimate simultaneous limits on $c_i^{\mathcal{L}}$, $c_i^{\mathcal{O}}$ and the translated limits on $c_i^{\mathcal{L}_g}$. We give an insight into the choice of beam polarizations in this process in Sec. III C and conclude in Sec. IV.

II. OBSERVABLES AND EFFECT OF BEAM POLARIZATIONS

We study W^+W^- production at ILC running at $\sqrt{s} = 500$ GeV and integrated luminosity $\mathcal{L} = 100$ fb^{-1} using longitudinal polarization of e^- and e^+ beams giving 50 fb^{-1} to each choice of beam polarization. The Feynman diagrams for the process are shown in Fig. 1 where Fig. 1(a) corresponds to the ν_e mediated t-channel diagram and Fig. 1(b) corresponds to the $V(Z/\gamma)$ mediated s-channel diagram containing the anomalous triple gauge boson couplings (aTGC) contributions represented by the shaded blob. The decay mode is chosen to be

$$W^+ \to q_u\bar{q}_d, \qquad W^- \to l^-\bar{\nu}_l, \qquad l = e, \mu, \tag{9}$$

where q_u and q_d are up-type and down-type quarks, respectively. We use complete set of eight spin-1 observables of W^- boson [6,7].

[2]We calculate the cross section up to $\mathcal{O}(\Lambda^{-4})$, i.e., quadratic in dimension-6 (as linear approximation is not valid, see Appendix B) and linear in dimension-8 couplings choosing dimension-8 couplings to be zero to compare our result with current LHC constraints on dimension-6 parameters [58,60].

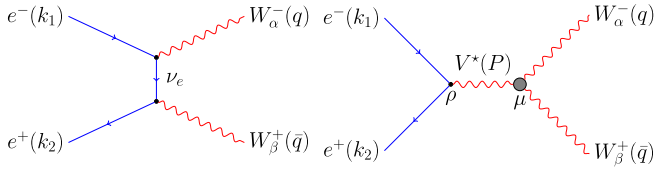

FIG. 1. Feynman diagrams of $e^+e^- \to W^+W^-$, (a) t channel and (b) s channel with anomalous W^+W^-V ($V = \gamma$, Z) vertex contribution shown by the shaded blob.

The W boson being a spin-1 particle, its normalized production density matrix in the spin basis can be written as [2,5]

$$\rho(\lambda,\lambda') = \frac{1}{3}\left[I_{3\times3} + \frac{3}{2}\vec{p}.\vec{S} + \sqrt{\frac{3}{2}}T_{ij}(S_iS_j + S_jS_i)\right], \quad (10)$$

where $\vec{p} = \{p_x, p_y, p_z\}$ is the vector polarization of a spin-1 particle, $\vec{S} = \{S_x, S_y, S_z\}$ is the spin basis, and $T_{ij}(i,j = x,y,z)$ is the second-rank symmetric traceless tensor, and λ and λ' are helicities of the particle. The tensor T_{ij} has five independent elements, which are T_{xy}, T_{xz}, T_{yz}, $T_{xx} - T_{yy}$, and T_{zz}. Combining the $\rho(\lambda,\lambda')$ with the normalized decay density matrix of the particle to a pair of fermion f, the differential cross section would be [5]

$$\begin{aligned}\frac{1}{\sigma}\frac{d\sigma}{d\Omega_f} = \frac{3}{8\pi}\Bigg[&\left(\frac{2}{3} - (1-3\delta)\frac{T_{zz}}{\sqrt{6}}\right) + \alpha p_z\cos\theta_f + \sqrt{\frac{3}{2}}(1-3\delta)T_{zz}\cos^2\theta_f + \left(\alpha p_x + 2\sqrt{\frac{2}{3}}(1-3\delta)T_{xz}\cos\theta_f\right)\sin\theta_f\cos\phi_f \\ &+ \left(\alpha p_y + 2\sqrt{\frac{2}{3}}(1-3\delta)T_{yz}\cos\theta_f\right)\sin\theta_f\sin\phi_f + (1-3\delta)\left(\frac{T_{xx}-T_{yy}}{\sqrt{6}}\right)\sin^2\theta_f\cos(2\phi_f) \\ &+ \sqrt{\frac{2}{3}}(1-3\delta)T_{xy}\sin^2\theta_f\sin(2\phi_f)\Bigg]. \end{aligned} \quad (11)$$

Here θ_f, ϕ_f are the polar and the azimuthal orientation of the fermion f, in the rest frame of the particle (W) with its would-be momentum along the z direction. The initial beam direction and the W^- momentum in the lab frame define the x-z plane, i.e., $\phi = 0$ plane, in the rest frame of W^- as well. In this case $\alpha = -1$ and $\delta = 0$. The vector polarizations $\vec{p}$ and independent tensor polarizations T_{ij} are calculable from the asymmetries constructed from the decay angular distribution of the lepton (here l^-). For example p_x can be calculated from the asymmetry A_x as

$$A_x = \frac{\sigma(\cos\phi_f > 0) - \sigma(\cos\phi_f < 0)}{\sigma(\cos\phi_f > 0) + \sigma(\cos\phi_f < 0)} \equiv \frac{3\alpha p_x}{4}. \quad (12)$$

The asymmetries corresponding to all other polarizations, vector polarizations p_y, p_z and independent tensor polarizations T_{ij} are A_y, A_z, A_{xy}, A_{xz}, A_{yz}, $A_{x^2-y^2}$, A_{zz}; see Ref. [7] for details.

Owing to the t-channel process [Fig. 1(a)] and absence of a u-channel process, like in ZV production [7,80], the $W^\pm$ produced are not forward-backward symmetric. We include the forward-backward asymmetry of W^-, defined as

$$A_{fb} = \frac{1}{\sigma_{W^+W^-}}\left[\int_0^1 \frac{d\sigma_{W^+W^-}}{d\cos\theta_{W^-}} - \int_{-1}^0 \frac{d\sigma_{W^+W^-}}{d\cos\theta_{W^-}}\right], \quad (13)$$

to the set of observables making a total of ten observables including the cross section as well. Here θ_{W^-} is the production angle of the W^- with respect to the e^- beam direction and $\sigma_{W^+W^-}$ is the production cross section.

These asymmetries can be measured in a real collider from the final state lepton l^-. One has to calculate the asymmetries in the rest frame of W^- which require the missing $\bar{\nu}_l$ momenta to be reconstructed. At an e^+ e^- collider, as studied here, reconstructing the missing $\bar{\nu}_l$ is possible because only one missing particle is involved and no parton distribution functions are involved, i.e., initial momenta are known. But for a collider where parton distribution functions are involved, reconstructing the actual missing momenta may not be possible.

We explore the dependence of the cross section and asymmetries on the longitudinal polarization η_3 of e^- and ξ_3 of e^+. In Fig. 2, we show the production cross section $\sigma_{W^+W^-}$ and A_x as a function of beam polarizations as an example. The cross section decreases along the $\eta_3 = -\xi_3$ path from 20 pb on the left-top corner to 7.2 pb at the unpolarized point and further to 1 pb in the right-bottom corner. This is because of the $W^\pm$ couples to the left chiral e^-; i.e., it requires e^- to be negatively polarized and e^+ to be positively polarized for the higher cross section. The variation of A_{fb} (not shown) with the beam polarization is the same as the cross section but very slow above the line $\eta_3 = \xi_3$. From this, we can expect that a positive η_3 and a negative ξ_3 will reduce the SM contributions to observables increasing the $S/\sqrt{B}$ ratio (S = signal, B = background). Some other asymmetries, like A_x, have the opposite dependence on the beam polarizations compared to the cross section; their modulus reduce for negative η_3 and positive ξ_3.

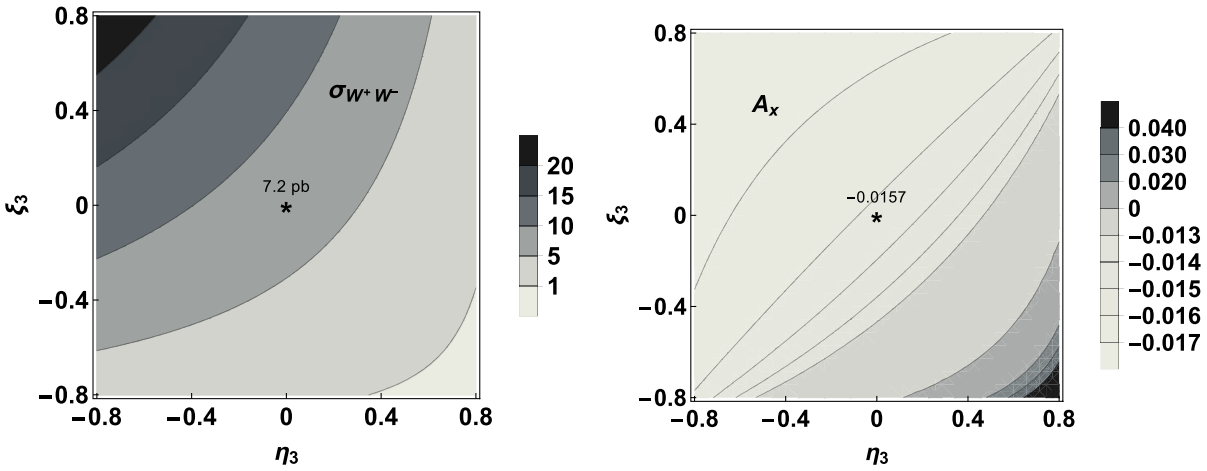

FIG. 2. The production cross section $\sigma_{W^+W^-}$ in pb (left panel) and the polarization asymmetry A_x (right panel) in the SM as a function of longitudinal beam polarizations η_3 (for e^-) and ξ_3 (for e^+) at $\sqrt{s} = 500$ GeV. The asterisks represent the unpolarized points and the numbers near them correspond to the SM values for corresponding observables with unpolarized beams.

III. PROBE TO THE ANOMALOUS COUPLINGS

The W^+W^-V vertex (Fig. 3) for the Lagrangian in Eq. (4) for on-shell Ws would be $ig_{WWV}\Gamma_V^{\mu\alpha\beta}$ [14,16] and it is given by

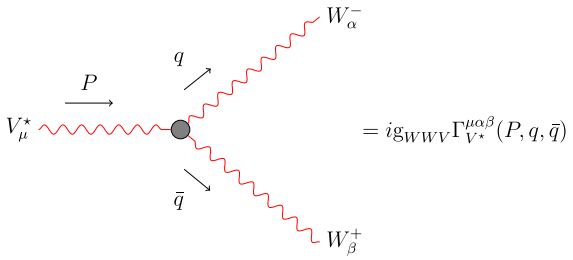

FIG. 3. The WWV vertex showing anomalous contribution represented by the shaded blob on top of SM. The momentum P is incoming to the vertex, while q and $\bar{q}$ are outgoing from the vertex.

$$\begin{aligned}\Gamma_V^{\mu\alpha\beta} &= f_1^V(q-\bar{q})^\mu g^{\alpha\beta} - \frac{f_2^V}{m_W^2}(q-\bar{q})^\mu P^\alpha P^\beta \\ &+ f_3^V(P^\alpha g^{\mu\beta} - P^\beta g^{\mu\alpha}) + if_4^V(P^\alpha g^{\mu\beta} + P^\beta g^{\mu\alpha}) \\ &+ if_5^V\epsilon^{\mu\alpha\beta\rho}(q-\bar{q})_\rho - f_6^V\epsilon^{\mu\alpha\beta\rho}P_\rho \\ &+ \frac{\widetilde{f_7^V}}{m_W^2}(\bar{q}^\alpha\epsilon^{\mu\beta\rho\sigma} + q^\beta\epsilon^{\mu\alpha\rho\sigma})q_\rho\bar{q}_\sigma, \end{aligned} \tag{14}$$

where P, q, $\bar{q}$ are the four-momenta of V, W^-, W^+, respectively. The momentum conventions are shown in Fig. 3. The form factors f_is have been obtained from the Lagrangian in Eq. (4) using FeynRules [96] to be

$$\begin{aligned} &f_1^V = g_1^V + \frac{\hat{s}}{2m_W^2}\lambda^V,\quad f_2^V = \lambda^V,\quad f_3^V = g_1^V + \kappa^V + \lambda^V,\quad f_4^V = g_4^V, \\ &f_5^V = g_5^V,\quad f_6^V = \widetilde{\kappa^V} + \left(1 - \frac{\hat{s}}{2m_W^2}\right)\widetilde{\lambda^V},\quad \widetilde{f_7^V} = \widetilde{\lambda^V}. \end{aligned} \tag{15}$$

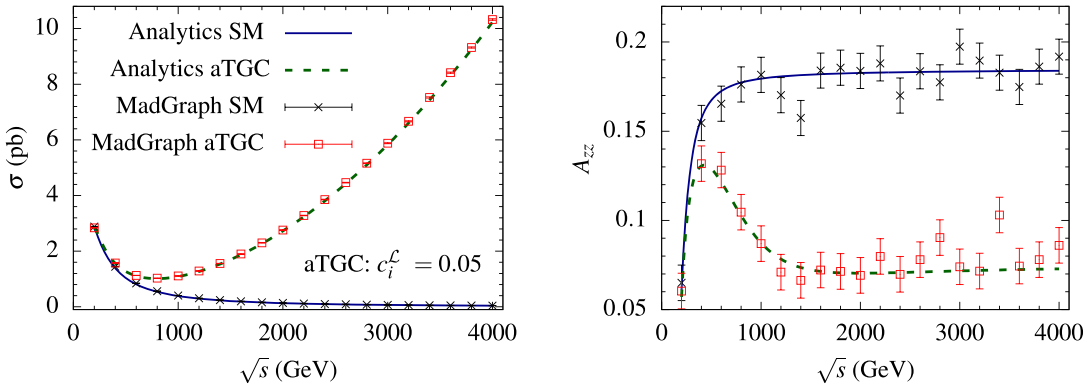

FIG. 4. The cross section σ including the decays in pb (left panel) and the asymmetry A_{zz} (right panel) in the SM and aTGC with all anomalous couplings ($c_i^{\mathcal{L}}$) at 0.05 as a function of $\sqrt{s}$ for the SM analytic (solid-blue) and aTGC analytic (dashed-green) with unpolarized beams. The *crossed* (black) points and *boxed* (red) points with the error bar correspond to results from MadGraph5. The error bars are given for number of events of 10^4.

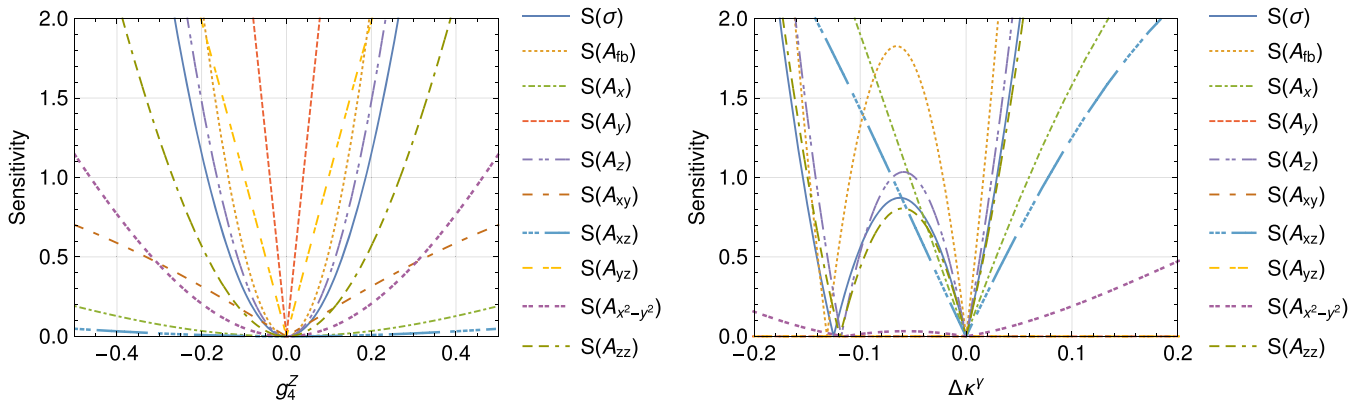

FIG. 5. The one parameter sensitivities of cross section σ, A_{fb} and the eight polarization asymmetries (A_i) on g_4^Z (left panel) and on $\Delta\kappa^\gamma$ (right panel) for $\sqrt{s} = 500$ GeV, $\mathcal{L} = 100$ fb^{-1} with unpolarized beams.

We use the vertex factors in Eq. (14) for the analytical calculation of our observables and cross validate them numerically with MadGraph5 [95] implementation of Eq. (4). As an example, we present two observables, $\sigma_{W^+W^-}$ and A_{zz}, for the SM ($c_i^{\mathcal{L}} = 0.0$) and for a chosen couplings point $c_i^{\mathcal{L}} = 0.05$, in Fig. 4. The agreement between the analytical and the numerical calculations over a range of $\sqrt{s}$ indicates the validity of relations in Eq. (15), especially the s dependence of f_1^V and f_6^V.

Analytical expressions of all the observables have been obtained and their dependence on the anomalous couplings $c_i^{\mathcal{L}}$ are given in Table V in Appendix A. The CP-even couplings in CP-even observables σ, A_x, A_z, A_{xz}, $A_{x^2-y^2}$, and A_{zz} appear in linear as well as in quadratic form but do not appear in the CP-odd observables A_y, A_{xy}, and A_{yz}. On the other hand, CP-odd couplings appear linearly in CP-odd observables and quadratically in CP-even observables. Thus, the CP-even couplings may have a double patch in their confidence interval, leading to asymmetric limits which will be discussed in Sec. III A. On the other hand, the CP-odd couplings will have a single patch in their confidence interval and will pose symmetric limits.

A. Sensitivity of observables on anomalous couplings and their binning

The sensitivity of an observable $\mathcal{O}$ depending on anomalous couplings $\vec{f}$ with beam polarization η_3, ξ_3 is given by

$$S\mathcal{O}(\vec{f},\eta_3,\xi_3) = \frac{|\mathcal{O}(\vec{f},\eta_3,\xi_3) - \mathcal{O}(\vec{0},\eta_3,\xi_3)|}{|\delta\mathcal{O}(\eta_3,\xi_3)|}, \quad (16)$$

where $\delta\mathcal{O} = \sqrt{(\delta\mathcal{O}_{\text{stat.}})^2 + (\delta\mathcal{O}_{\text{sys.}})^2}$ is the estimated error in $\mathcal{O}$. The error for the cross section would be

$$\delta\sigma(\eta_3,\xi_3) = \sqrt{\frac{\sigma(\eta_3,\xi_3)}{\mathcal{L}} + \varepsilon_\sigma^2\sigma(\eta_3,\xi_3)^2} \quad (17)$$

whereas the estimated error in the asymmetries would be

$$\delta A(\eta_3,\xi_3) = \sqrt{\frac{1 - A(\eta_3,\xi_3)^2}{\mathcal{L}\sigma(\eta_3,\xi_3)} + \varepsilon_A^2}. \quad (18)$$

Here $\mathcal{L}$ is the luminosity of the data set, and ε_σ and ε_A are the systematic fractional errors in the cross section and asymmetries, respectively. We take $\mathcal{L} = 50$ fb^{-1} for each choice of beam polarizations, $\varepsilon_\sigma = 2\%$ and $\varepsilon_A = 1\%$, as a benchmark scenario for the present analyses. The sensitivity of all 10 observables have been studied on all 14 couplings of the Lagrangian in Eq. (4) with the chosen $\sqrt{s}$, $\mathcal{L}$ and systematic uncertainties. The sensitivity of all observables on g_4^Z and $\Delta\kappa^\gamma$ are shown in Fig. 5 as representative. Being CP odd (either only linear or only quadratic terms present), g_4^Z has a single patch in the confidence interval, while $\Delta\kappa^\gamma$, being CP even (linear as well as quadratic terms present), has two patches in the sensitivity curve, as noted earlier. The CP-odd observable A_y provides the tightest one parameter limit on g_4^Z. The tightest 1σ limit on $\Delta\kappa^\gamma$ is obtained using A_{fb}, while at 2σ level, a combination of A_{fb} and A_x provide the tightest limit.

Here, we have a total of 14 different anomalous couplings to be measured, while we only have 10 observables. A certain combination of large couplings may mimic the SM within the statistical errors. To avoid these, we need more observables to be included in the analysis. We achieve this by dividing $\cos\theta_{W^-}$ into eight bins and calculate the cross section and polarization asymmetries in all of them. In Fig. 6, the cross section and the polarization asymmetries A_z, A_x, and A_y are shown as a function of $\cos\theta_{W^-}$ for the SM and some aTGC couplings for both polarized and unpolarized beams. The SM values for unpolarized case are shown in dotted (blue) lines, and the SM values with a polarization of $(\eta_3,\xi_3) = (+0.6,-0.6)$ are shown in dashed (black) lines. The solid (red) lines correspond to unpolarized aTGC values, while dashed-dotted (green)

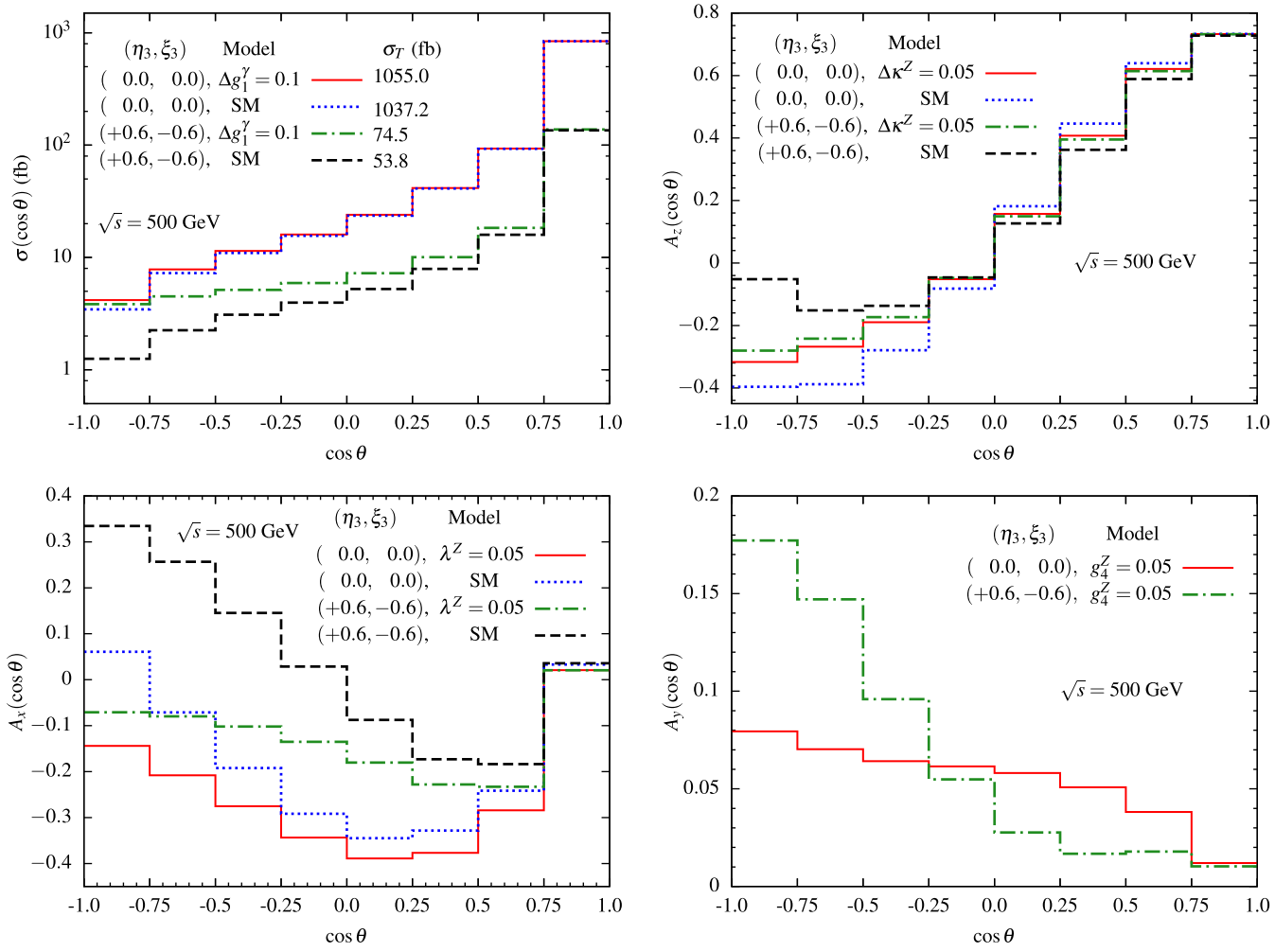

FIG. 6. The cross section σ (left-top), A_z (right-top), A_x (left-bottom) and A_y (right-bottom) as a function of $\cos\theta$ of W^- in 8 bins for $\sqrt{s} = 500$ GeV. The dotted (blue) lines correspond to the SM unpolarized values, solid (red) lines correspond to the unpolarized aTGC values, dashed (black) lines represent polarized SM values, and dashed-dotted (green) lines represent polarized aTGC vzalues of observables. For aTGC, only one anomalous coupling has been assumed nonzero and others kept at zero in each panel.

lines represent polarized aTGC values of observables. For the cross section (left-top panel), we take Δg_1^γ to be 0.1 and all other couplings to zero for both polarized and unpolarized beams. We see that the fractional deviation from the SM value is larger in the most backward bin $[\cos\theta_{W^-} \in (-1.0, -0.75)]$ and gradually reduces in the forward direction. The deviation is even larger in the case of beam polarization. The sensitivity of the cross section on Δg_1^γ is thus expected to be high in the most backward bin. In the case of asymmetries, A_z (right-top panel), A_{xz} (left-bottom panel), and A_y (right-bottom panel), the aTGC are assumed to be $\Delta\kappa^Z = 0.05$, $\lambda^Z = 0.05$ and $g_4^Z = 0.05$, respectively, while others are kept at zero. The changes in the asymmetries due to aTGC are larger in the backward bin for both polarized and unpolarized beam cases. We note that the asymmetries may not have the highest sensitivity in the most backward bin but in some other bin. We consider the cross section and eight polarization asymmetries in all eight bins; i.e., we have 72 observables in our analysis.

One parameter sensitivity of the set of nine observables in all eight bins have been studied. We show the sensitivity of A_y on g_4^Z and of A_z on $\Delta\kappa^\gamma$ in the eight bins in Fig. 7 as representative. The tightest limits based on sensitivity (coming from one bin) is roughly twice as tight as compared to the unbinned case in Fig. 5. Thus, we expect simultaneous limits on all the couplings to be tighter when using binned observables.

We perform a set of Markov-chain Monte Carlo (MCMC) analyses with a different set of observables for different kinematical cuts with unpolarized beams to understand their roles in providing limits on the anomalous couplings. These analyses are listed in Table II. The corresponding 14-dimensional rectangular

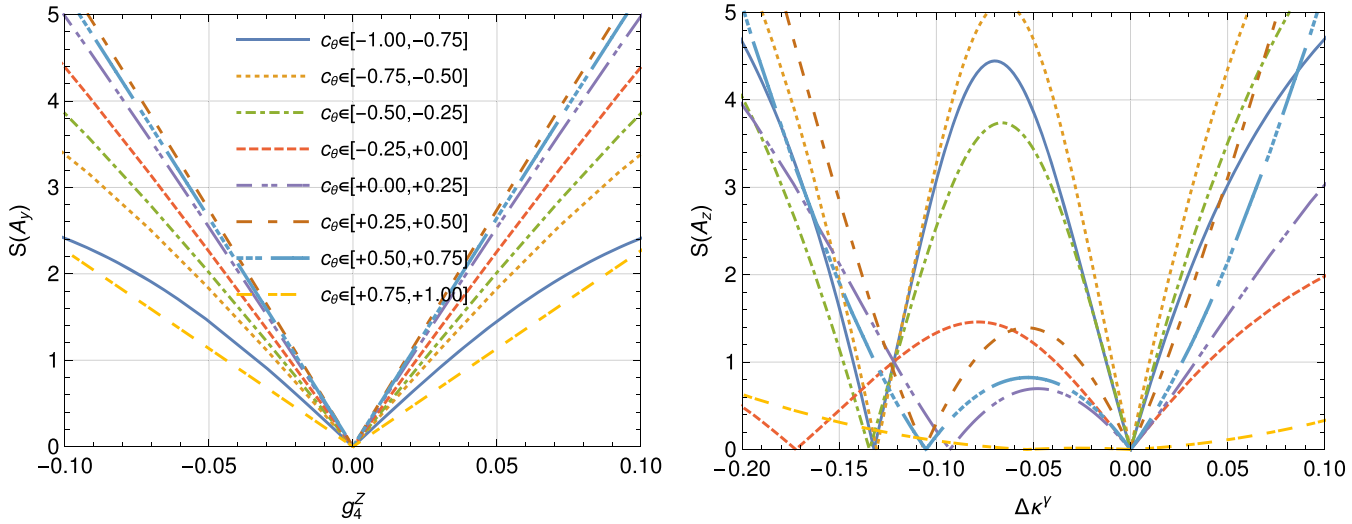

FIG. 7. The one parameter sensitivities of A_x on g_4^Z (left panel) and of A_z on $\Delta\kappa^\gamma$ (right panel) in eight bins at $\sqrt{s} = 500$ GeV, $\mathcal{L} = 100$ fb^{-1} with $c_\theta = \cos\theta_{W^-}$ for unpolarized beams.

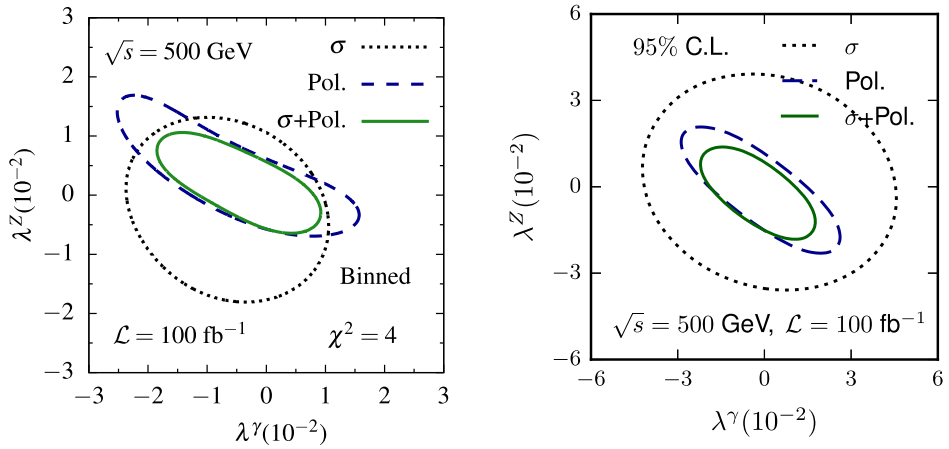

FIG. 8. The $\chi^2 = 4$ contours in the left panel and 95% C.L. contours from the simultaneous analysis in the right panel in the λ^γ-λ^Z plane using the binned cross sections (σ) alone in dotted (black) lines, just binned polarizations asymmetries (Pol.) in dashed (blue) lines, and the binned cross sections together with binned polarization asymmetries (σ + Pol.) in solid (green) lines for $\sqrt{s} = 500$ GeV, $\mathcal{L} = 100$ fb^{-1}.

volume[3] made out of 95% Bayesian confidence interval (BCI) on the anomalous couplings are also listed in Table II in the last column. The simplest analysis would be to consider only the cross section in the full $\cos\theta_{W^-}$ domain and perform MCMC analysis which is named as σ-unbinned. The typical 95% limits on the parameters range from $\sim \pm 0.04$ to ± 0.25 giving the volume of limits to be 4.4×10^{-11}. As we have polarizations asymmetries, the straight forward analysis would be to consider all the observables for the full domain of $\cos\theta_{W^-}$. This analysis is named Unbinned where limits on anomalous couplings get constrained better by reducing the volume of limits by a factor of 10 compared to the σ-unbinned. To see how binning improves the limits, we perform an analysis named σ-binned using only the cross section in eight bins. We see that the analysis σ-binned is better than the σ-unbinned and comparable to the analysis Unbinned. To see the strength of the polarization asymmetries, we perform an analysis named Pol.-binned using just the polarization asymmetries in 8 bins. We see that this analysis is much better than the analysis σ-binned.

[3]This volume of limit is the volume of a 14-dimensional rectangular box bounding by the 95% BCI projection of simultaneous limits in each coupling, which can be a measure of goodness of the benchmark beam polarization. We computed the cross section and other asymmetries keeping term up to quadratic in couplings. In this case, even a single observable can give a finite volume of limit and constrain all 14 couplings, which would not be possible if only terms linear in couplings were present.

TABLE II. The list of analyses performed in the present work and set of observables used with different kinematical cuts to obtain simultaneous limits on the anomalous couplings at $\sqrt{s} = 500$ GeV, $\mathcal{L} = 100$ fb^{-1} with unpolarized beams. The rectangular volumes of couplings at 95% BCI are shown in the last column for each analyses (see text for details).

Analysis name	Set of observables	Kinematical cut on $\cos\theta_{W^-}$	Volume of limits
σ-unbinned	σ	$\cos\theta_{W^-} \in [-1.0, 1.0]$	4.4×10^{-11}
Unbinned	σ, A_{fb}, A_i	$\cos\theta_{W^-} \in [-1.0, 1.0]$	3.1×10^{-12}
σ-binned	σ	$\cos\theta_{W^-} \in [\frac{m-5}{4}, \frac{m-4}{4}]$, $m = 1, 2, \ldots, 8$	3.7×10^{-12}
Pol.-binned	A_i	$\cos\theta_{W^-} \in [\frac{m-5}{4}, \frac{m-4}{4}]$, $m = 1, 2, \ldots, 8$	1.6×10^{-15}
Binned	σ, A_i	$\cos\theta_{W^-} \in [\frac{m-5}{4}, \frac{m-4}{4}]$, $m = 1, 2, \ldots, 8$	5.2×10^{-17}

The most natural and complete analysis would be to consider all the observables after binning. The analysis is named as Binned which has limits much better than any analysis. The comparison between the analyses, σ-binned, Pol.-binned, and Binned, is shown in Fig. 8 in the panel λ^γ-λ^Z in two-parameter (left panel) as well as in multiparameter (right panel) analysis using MCMC as representative. The right panel reflects Table II. The behaviors are same even in the two-parameter analysis (left panel) by keeping all other parameters to zero; i.e., the bounded region for $\chi^2 = 4$ is smaller in Pol.-binned (Pol.) than σ-binned (σ) and smallest for Binned ($\sigma +$ Pol.).

We also calculate one-parameter limits on all the couplings at 95% C.L. considering all the binned observables with unpolarized beams in the effective vertex formalism as well as in the effective operator approach and list them in the last column of Tables III and IV, respectively, for comparison. In the next subsection, we study the effect of beam polarizations on the limits of the anomalous couplings.

B. Effect of beam polarizations to the limits on the anomalous couplings

We perform a MCMC analysis to estimate simultaneous limits on the anomalous couplings using the binned observables in both effective vertex formalism with 14 independent couplings and an effective operator approach with five independent couplings for a set of chosen beam polarizations (η_3, ξ_3) to be (0, 0), $(+0.2, -0.2)$, $(+0.4, -0.4)$, $(+0.6, -0.6)$, $(+0.8, -0.6)$, $(+0.8, -0.8)$ along

TABLE III. List of posterior 95% BCI of anomalous couplings $c_i^{\mathcal{L}}$ (10^{-2}) of the Lagrangian in Eq. (4) at $\sqrt{s} = 500$ GeV, $\mathcal{L} = 100$ fb^{-1} for a chosen set of longitudinal beam polarizations η_3 and ξ_3 from MCMC global fits in the Binned case. The limits for the best choice of beam polarization within technological reach, i.e., $(\pm 0.8, \mp 0.6)$ are marked in **bold**. The pictorial visualizations for these 95% BCI of $c_i^{\mathcal{L}}$ are shown in Fig. 9 in the left panel. The one-parameter ($1P$) limits (10^{-2}) at 95% BCI with unpolarized beams are given in the last column for comparison. The notation used here is $^{\text{high}}_{\text{low}} \equiv [\text{low}, \text{high}]$ with low being the lower limit and high being the upper limit.

Parameter	(0, 0)	$(\pm 0.2, \mp 0.2)$	$(\pm 0.4, \mp 0.4)$	$(\pm 0.6, \mp 0.6)$	$(\pm \mathbf{0.8}, \mp \mathbf{0.6})$	$(\pm 0.8, \mp 0.8)$	$1P(0, 0)$
Δg_1^γ	$^{+5.5}_{-8.5}$	$^{+3.3}_{-7.4}$	$^{+2.7}_{-6.0}$	$^{+2.1}_{-2.7}$	$^{\mathbf{+1.7}}_{\mathbf{-2.3}}$	$^{+1.6}_{-2.0}$	$^{+1.3}_{-1.4}$
g_4^γ	$^{+5.8}_{-6.0}$	$^{+5.3}_{-5.4}$	$^{+4.0}_{-4.0}$	$^{+3.0}_{-3.0}$	$^{\mathbf{+2.5}}_{\mathbf{-2.5}}$	$^{+2.2}_{-2.2}$	$^{+1.9}_{-1.9}$
g_5^γ	$^{+6.1}_{-6.1}$	$^{+5.1}_{-5.2}$	$^{+2.6}_{-3.1}$	$^{+1.4}_{-2.0}$	$^{\mathbf{+1.1}}_{\mathbf{-1.6}}$	$^{+1.0}_{-1.4}$	$^{+1.9}_{-2.0}$
λ^γ	$^{+1.4}_{-1.8}$	$^{+1.2}_{-1.6}$	$^{+1.2}_{-1.2}$	$^{+1.0}_{-0.68}$	$^{\mathbf{+0.89}}_{\mathbf{-0.61}}$	$^{+0.81}_{-0.57}$	$^{+0.77}_{-1.1}$
$\tilde{\lambda}^\gamma$	$^{+1.6}_{-1.6}$	$^{+1.4}_{-1.4}$	$^{+1.1}_{-1.1}$	$^{+0.88}_{-0.88}$	$^{\mathbf{+0.82}}_{\mathbf{-0.82}}$	$^{+0.77}_{-0.78}$	$^{+1.0}_{-1.0}$
$\Delta\kappa^\gamma$	$^{+0.91}_{-5.7}$	$^{+0.32}_{-4.4}$	$^{+0.46}_{-4.3}$	$^{+0.28}_{-0.69}$	$^{\mathbf{+0.27}}_{\mathbf{-0.55}}$	$^{+0.25}_{-0.48}$	$^{+0.33}_{-0.34}$
$\tilde{\kappa}^\gamma$	$^{+6.1}_{-6.0}$	$^{+5.2}_{-5.2}$	$^{+4.0}_{-3.9}$	$^{+2.9}_{-3.0}$	$^{\mathbf{+2.6}}_{\mathbf{-2.6}}$	$^{+2.3}_{-2.3}$	$^{+2.3}_{-2.4}$
Δg_1^Z	$^{+7.2}_{-3.7}$	$^{+5.6}_{-2.8}$	$^{+4.5}_{-2.6}$	$^{+2.1}_{-2.0}$	$^{\mathbf{+1.8}}_{\mathbf{-1.7}}$	$^{+1.6}_{-1.5}$	$^{+1.3}_{-1.3}$
g_4^Z	$^{+4.8}_{-4.7}$	$^{+4.3}_{-4.3}$	$^{+3.3}_{-3.3}$	$^{+2.5}_{-2.5}$	$^{\mathbf{+2.2}}_{\mathbf{-2.2}}$	$^{+2.0}_{-2.0}$	$^{+1.4}_{-1.4}$
g_5^Z	$^{+4.7}_{-4.8}$	$^{+4.0}_{-4.1}$	$^{+2.1}_{-2.3}$	$^{+1.3}_{-1.5}$	$^{\mathbf{+1.0}}_{\mathbf{-1.3}}$	$^{+0.86}_{-1.2}$	$^{+1.2}_{-1.3}$
λ^Z	$^{+1.1}_{-1.5}$	$^{+1.0}_{-1.3}$	$^{+0.80}_{-1.1}$	$^{+0.49}_{-0.94}$	$^{\mathbf{+0.47}}_{\mathbf{-0.83}}$	$^{+0.44}_{-0.76}$	$^{+0.56}_{-0.57}$
$\tilde{\lambda}^Z$	$^{+1.3}_{-1.3}$	$^{+1.1}_{-1.1}$	$^{+0.90}_{-0.90}$	$^{+0.77}_{-0.77}$	$^{\mathbf{+0.73}}_{\mathbf{-0.73}}$	$^{+0.68}_{-0.68}$	$^{+0.57}_{-0.56}$
$\Delta\kappa^Z$	$^{+3.6}_{-1.5}$	$^{+3.2}_{-0.49}$	$^{+3.1}_{-0.44}$	$^{+0.56}_{-0.38}$	$^{\mathbf{+0.43}}_{\mathbf{-0.35}}$	$^{+0.36}_{-0.32}$	$^{+0.43}_{-0.48}$
$\tilde{\kappa}^Z$	$^{+4.7}_{-5.0}$	$^{+4.2}_{-4.2}$	$^{+3.3}_{-3.3}$	$^{+2.5}_{-2.5}$	$^{\mathbf{+2.2}}_{\mathbf{-2.2}}$	$^{+2.1}_{-2.0}$	$^{+1.5}_{-1.5}$

TABLE IV. The list of posterior 95% BCI of anomalous couplings $c_i^{\mathcal{O}}$ (TeV^{-2}) of effective operators in Eq. (2) and their translated limits on the couplings $c_i^{\mathcal{L}_g}$ (10^{-2}) for $\sqrt{s} = 500$ GeV, $\mathcal{L} = 100$ fb^{-1} in the Binned case for a chosen set of longitudinal beam polarizations η_3 and ξ_3 from MCMC global fits. The pictorial visualizations for these 95% BCI of $c_i^{\mathcal{O}}$ and $c_i^{\mathcal{L}_g}$ are shown in Fig. 9 in the right-top and right-bottom panels, respectively. The rest of the details are same as in Table III.

Parameters	(0, 0)	($\pm$0.2, $\mp$0.2)	($\pm$0.4, $\mp$0.4)	($\pm$0.6, $\mp$ 0.6)	($\pm$**0.8**, $\mp$**0.6**)	($\pm$0.8, $\mp$0.8)	$1P(0,0)$
$\frac{c_{WWW}}{\Lambda^2}$	$^{+1.3}_{-1.9}$	$^{+1.2}_{-1.4}$	$^{+1.2}_{-1.1}$	$^{+1.1}_{-0.96}$	$^{\mathbf{+1.1}}_{\mathbf{-1.0}}$	$^{+1.0}_{-0.94}$	$^{+0.84}_{-0.97}$
$\frac{c_W}{\Lambda^2}$	$^{+5.0}_{-1.4}$	$^{+4.6}_{-1.1}$	$^{+0.83}_{-0.86}$	$^{+0.58}_{-0.72}$	$^{\mathbf{+0.60}}_{\mathbf{-0.73}}$	$^{+0.55}_{-0.63}$	$^{+0.55}_{-0.58}$
$\frac{c_B}{\Lambda^2}$	$^{+2.7}_{-23.7}$	$^{+1.9}_{-20.2}$	$^{+0.98}_{-1.3}$	$^{+0.62}_{-0.75}$	$^{\mathbf{+0.56}}_{\mathbf{-0.64}}$	$^{+0.47}_{-0.53}$	$^{+1.2}_{-1.3}$
$\frac{c_{W\tilde{W}W}}{\Lambda^2}$	$^{+1.4}_{-1.4}$	$^{+1.1}_{-1.1}$	$^{+0.97}_{-0.97}$	$^{+0.94}_{-0.93}$	$^{\mathbf{+0.91}}_{\mathbf{-0.90}}$	$^{+0.87}_{-0.87}$	$^{+0.97}_{-0.98}$
$\frac{c_{\tilde{W}}}{\Lambda^2}$	$^{+2.1}_{-12.0}$	$^{+9.8}_{-10.0}$	$^{+6.6}_{-6.7}$	$^{+4.2}_{-4.1}$	$^{\mathbf{+3.2}}_{\mathbf{-3.2}}$	$^{+2.6}_{-2.6}$	$^{+10.1}_{-9.9}$
λ^V	$^{+0.52}_{-0.79}$	$^{+0.50}_{-0.58}$	$^{+0.49}_{-0.46}$	$^{+0.46}_{-0.40}$	$^{\mathbf{+0.45}}_{\mathbf{-0.41}}$	$^{+0.42}_{-0.39}$	$^{+0.35}_{-0.40}$
$\widetilde{\lambda^V}$	$^{+0.60}_{-0.60}$	$^{+0.44}_{-0.45}$	$^{+0.40}_{-0.40}$	$^{+0.39}_{-0.38}$	$^{\mathbf{+0.37}}_{\mathbf{-0.37}}$	$^{+0.36}_{-0.36}$	$^{+0.40}_{-0.41}$
$\Delta\kappa^\gamma$	$^{+0.52}_{-6.4}$	$^{+0.44}_{-5.1}$	$^{+0.28}_{-0.38}$	$^{+0.24}_{-0.32}$	$^{\mathbf{+0.25}}_{\mathbf{-0.32}}$	$^{+0.23}_{-0.28}$	$^{+0.56}_{-0.61}$
$\widetilde{\kappa^\gamma}$	$^{+3.9}_{-3.9}$	$^{+3.2}_{-3.2}$	$^{+2.1}_{-2.1}$	$^{+1.3}_{-1.3}$	$^{\mathbf{+1.0}}_{\mathbf{-1.0}}$	$^{+0.84}_{-0.84}$	$^{+3.2}_{-3.2}$
Δg_1^Z	$^{+2.1}_{-0.59}$	$^{+1.9}_{-0.45}$	$^{+0.34}_{-0.36}$	$^{+0.24}_{-0.30}$	$^{\mathbf{+0.25}}_{\mathbf{-0.30}}$	$^{+0.23}_{-0.26}$	$^{+0.23}_{-0.24}$
$\Delta\kappa^Z$	$^{+3.6}_{-0.73}$	$^{+3.2}_{-0.45}$	$^{+0.34}_{-0.33}$	$^{+0.21}_{-0.24}$	$^{\mathbf{+0.21}}_{\mathbf{-0.24}}$	$^{+0.19}_{-0.20}$	$^{+0.30}_{-0.30}$
$\widetilde{\kappa^Z}$	$^{+1.1}_{-1.1}$	$^{+0.92}_{-0.91}$	$^{+0.62}_{-0.61}$	$^{+0.38}_{-0.38}$	$^{\mathbf{+0.29}}_{\mathbf{-0.30}}$	$^{+0.24}_{-0.24}$	$^{+0.92}_{-0.93}$

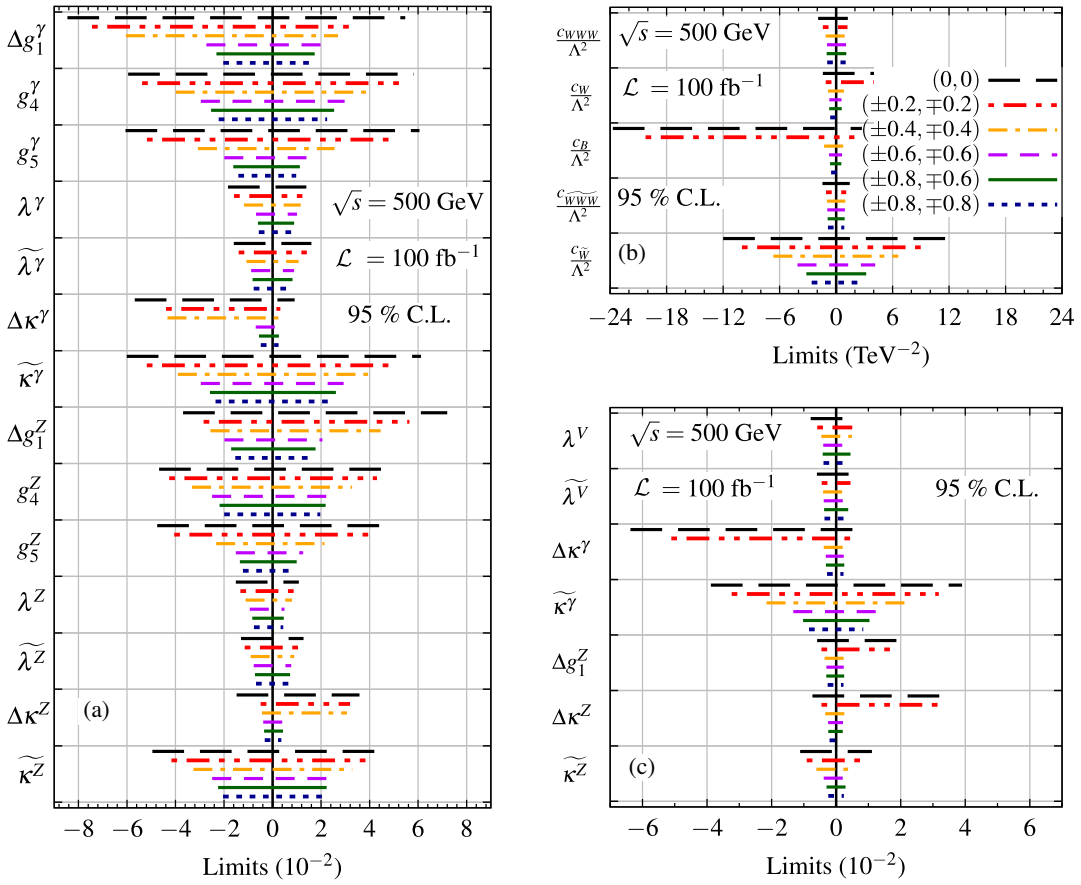

FIG. 9. The pictorial visualizations of 95% BCI limits obtained from MCMC global fits (a): on the anomalous couplings $c_i^{\mathcal{L}}$ in the left panel, (b): on $c_i^{\mathcal{O}}$ in the right-top panel and (c): on $c_i^{\mathcal{L}_g}$ in the right-bottom panel for $\sqrt{s} = 500$ GeV, $\mathcal{L} = 100$ fb^{-1} using the binned observables. The numerical values of the limits can be read of in Tables III and IV.

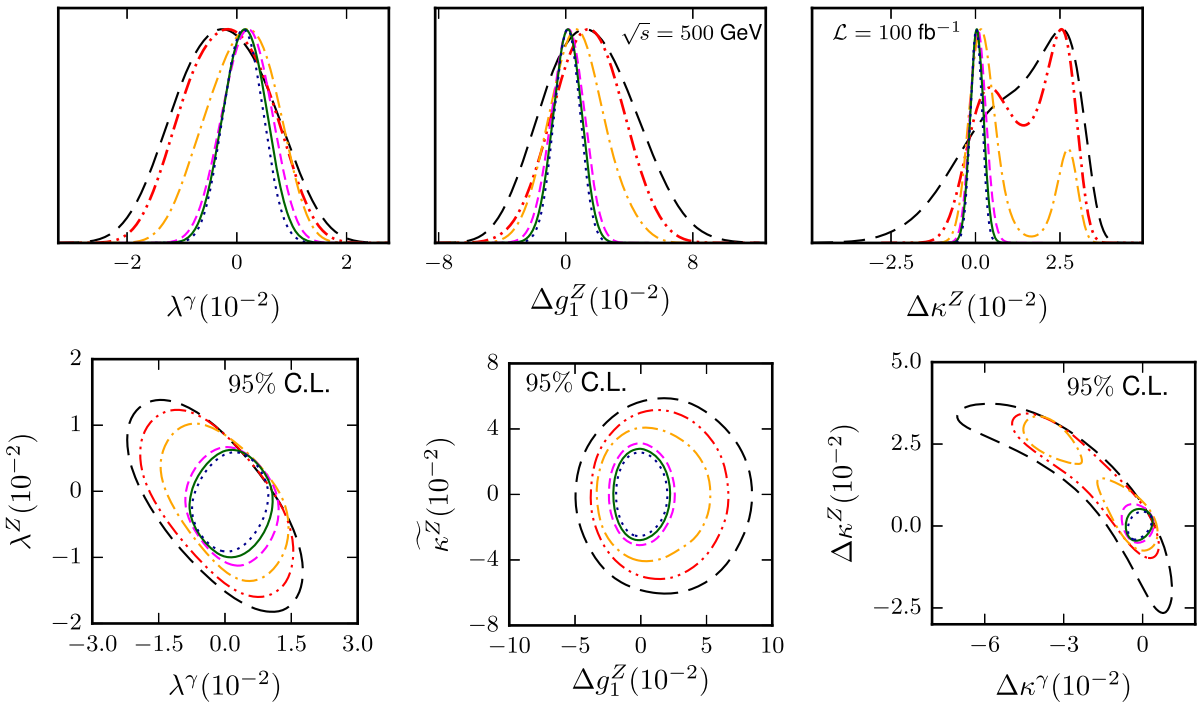

FIG. 10. The marginalized 1D projections for the couplings λ^γ, Δg_1^Z and $\Delta\kappa^Z$ in the top panel and 2D projections at 95% C.L. on λ^γ-λ^Z, Δg_1^Z-$\widetilde{\kappa}^Z$, and $\Delta\kappa^\gamma$-$\Delta\kappa^Z$ planes in the bottom panel from MCMC for a set of choice of beam polarizations are shown for $\sqrt{s} = 500$ GeV, $\mathcal{L} = 100$ fb^{-1} using the binned observables in the effective vertex formalism. The legend labels are same as in Figs. 9 and 11.

with their opposite values. The beam polarization $(+\eta_3, +\xi_3)$ and its opposite $(-\eta_3, -\xi_3)$ are combined at the level of χ^2 as

$$\chi^2_{\rm tot}(\pm\eta_3, \pm\xi_3) = \sum_{bin}\sum_{N}(\chi^2[\mathcal{O}_N(+\eta_3, +\xi_3)] + \chi^2[\mathcal{O}_N(-\eta_3, -\xi_3)]), \quad (19)$$

where N runs over all the observables. The 95% BCI simultaneous limits for the chosen set of beam polarizations combined according to Eq. (19) are shown in Table III for effective vertex formalism ($c_i^{\mathcal{L}}$) and in Table IV for effective operator approach ($c_i^{\mathcal{O}}$). The corresponding translated limit to the vertex factor couplings $c_i^{\mathcal{L}_g}$ are also shown in the Table IV using relation from Eq. (5). While presenting limits the following notation is used

$$^{\rm high}_{\rm low} \equiv [\rm low, high]$$

with low being lower limit and high being upper limit. A pictorial visualization of the limits shown in Table III and IV is given in Fig. 9 for the easy comparisons. The limits on the couplings get tighter as the magnitude of the beam polarizations are increased along $\eta_3 = -\xi_3$ path and become tightest at the extreme beam polarization $(\pm 0.8, \mp 0.8)$. However, the choice $(\pm 0.8, \mp 0.6)$ is best to put constraints on the couplings within the technological reach [97,98].

To show the effect of beam polarizations the marginalised 1D projection for the couplings λ^γ, Δg_1^Z and $\Delta\kappa^Z$ as well as 2D projection at 95% C.L. on λ^γ-λ^Z, Δg_1^Z-$\widetilde{\kappa}^Z$ and $\Delta\kappa^\gamma$-$\Delta\kappa^Z$ planes are shown in Fig. 10 for the effective vertex formalism ($c_i^{\mathcal{L}}$) as representative. We observe that as the magnitude of beam polarizations are increased from (0,0) to $(\pm 0.8, \mp 0.8)$ the contours get smaller centered around the SM values in the 2D projection which is reflected in the 1D projection as well. In the $\Delta\kappa^\gamma$-$\Delta\kappa^Z$ panel, the contours get divided into two part at $(\pm 0.4, \mp 0.4)$ and become one single contour later centered around the SM values. In the case of effective operator approach ($c_i^{\mathcal{O}}$), all the 1D and 2D (95% C.L.) projections after marginalization are shown in Fig. 11. In this case the couplings c_W and c_B has two patches up-to beam polarization $(\pm 0.2, \mp 0.2)$ and become one single patch starting at beam polarization $(\pm 0.3, \mp 0.3)$ centered around the SM values. As the magnitude of beam polarizations are increased along the $\eta_3 = -\xi_3$ line the measurement of the anomalous couplings gets improved. The set of beam polarizations chosen here are mostly along $\eta_3 = -\xi_3$ line, but some choices off to the line might provide the same results. A discussion on the choice of beam polarization is given in the next subsection.

C. On the choice of beam polarizations

In the previous subsection, we found that $(\pm\eta_3, \pm\xi_3) = (\pm 0.8, \pm 0.6)$ is the best choice of beam polarizations to

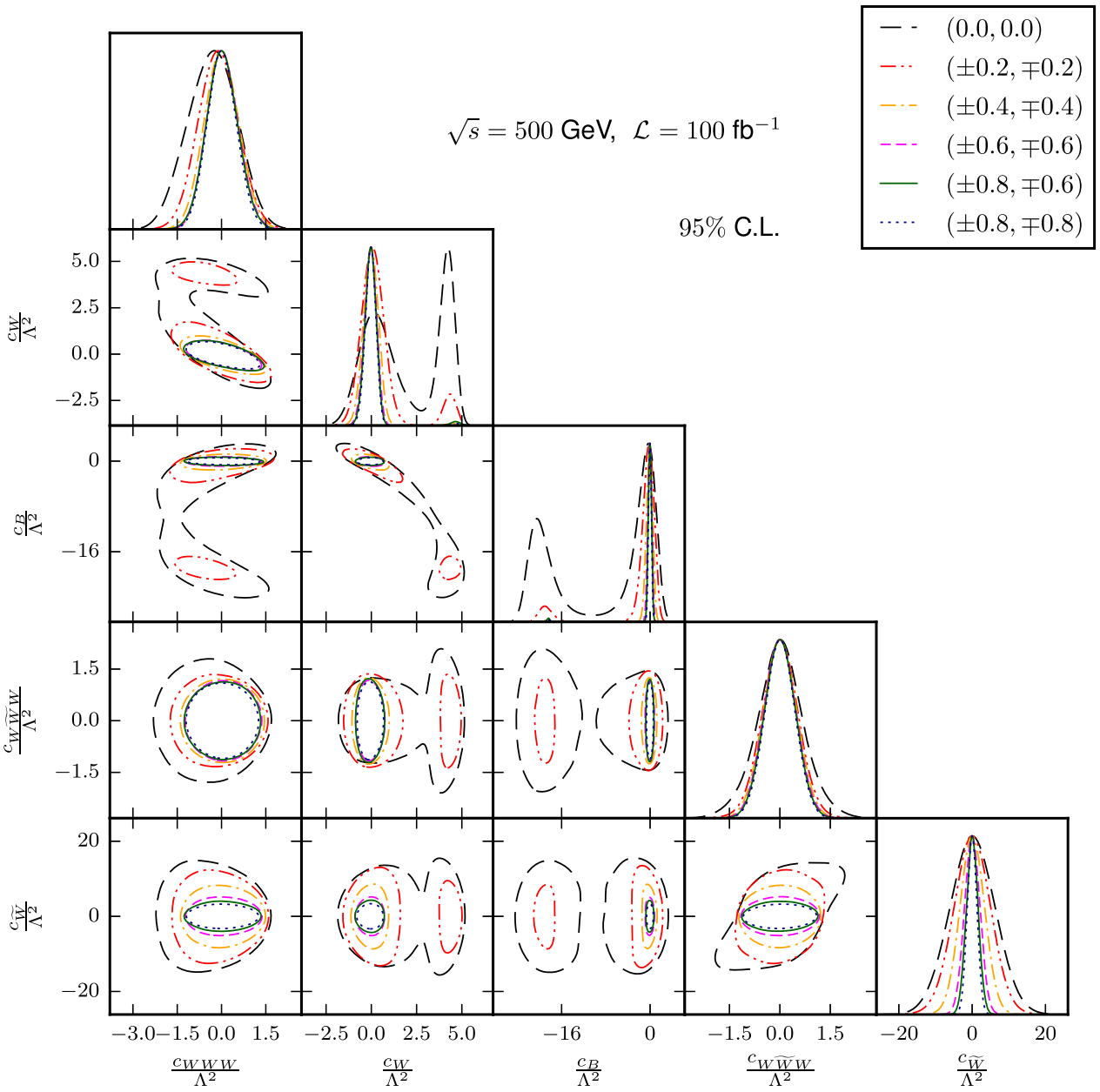

FIG. 11. All the marginalized 1D projections and 2D projections at 95% C.L. from the MCMC in a triangular array for the effective operators (TeV^{-2}) for a set of choices of beam polarizations for $\sqrt{s} = 500$ GeV, $\mathcal{L} = 100$ fb^{-1} using the binned observables.

provide simultaneous limits on the anomalous couplings obtained by MCMC analysis. Here, we discuss the average likelihood or the weighted volume of the parameter space defined as [80]

$$L(V_{\vec{f}}; \eta_3, \xi_3) = \int_{V_{\vec{f}}} \exp\left[-\frac{1}{2}\chi^2_{\text{tot}}(\vec{f}, \eta_3, \xi_3)\right] d\vec{f} \qquad (20)$$

to cross-examine the beam polarization choices made in the previous section. Here $\vec{f}$ is the coupling vector and $V_{\vec{f}}$ is the volume of parameter space over which the average is done and $L(V_{\vec{f}}; \eta_3, \xi_3)$ corresponds to the volume of the parameter space that is statistically consistent with the SM. One naively expects the limits to be tightest when $L(V_{\vec{f}}; \eta_3, \xi_3)$ is minimum. We calculate the above quantity as a function of $(\pm\eta_3, \pm\xi_3)$ for the Binned case in the effective vertex formalism given in the Lagrangian in Eq. (4) and present it in Fig. 12. As the opposite beam polarizations are combined, only the half-portions are shown in the η_3-ξ_3 plane. The dot (•) points along the $\eta_3 = -\xi_3$ are the chosen choice of beam polarizations for the MCMC analysis. We see that the average likelihood decreases along the $\eta_3 = -\xi_3$ line while it increases along the $\eta_3 = \xi_3$ line. The constant lines or contours of average

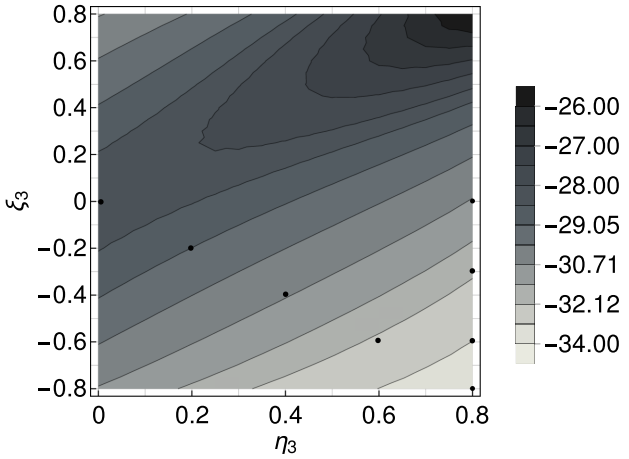

FIG. 12. The averaged likelihood $L_{Av} = L(V_{\vec{f}}; \eta_3, \xi_3)$ in log scale as a function of $(\pm\eta_3, \pm\xi_3)$ in the effective vertex formalism for $\sqrt{s} = 500$ GeV, $\mathcal{L} = 100$ fb^{-1}.

likelihood in the figure imply that any beam polarizations along the lines/contours will provide the similar shape of 1D and 2D projections of couplings and their limits. For example, the point $(\pm 0.8, \mp 0.6)$ is equivalent to the point $(\pm 0.7, \mp 0.7)$ as well as $(\pm 0.6, \pm 0.8)$ roughly in providing simultaneous limits which are verified from the limits obtained by the MCMC analysis. From the figure, it is clear that the polarization $(\pm 0.8, \mp 0.6)$ is indeed the best choice to provide simultaneous limits on the anomalous couplings within the achievable range. However, the plan for polarization choices are $(\eta_3, \xi_3) = (0, 0)$, $(\pm 0.8, 0)$, $(\pm 0.8, \mp 0.3)$, and $(\pm 0.8, \mp 0.6)$ at the ILC [99,100]. These off-diagonal choices are equivalent to the diagonal choices we have used as Fig. 12 indicates. The polarization choice $(\pm 0.8, 0)$ is equivalent to $(\pm 0.4, \mp 0.4)$ in providing limits on the couplings, while $(\pm 0.8, \mp 0.3)$ is equivalent to $(\pm 0.6, \mp 0.6)$ [$(\pm 0.57, \mp 0.57)$ to be precise]. For completeness we also show the limits on the couplings for the off-diagonal polarization choices $(\pm 0.8, 0)$ and $(\pm 0.8, \mp 0.3)$ in Table VI on column 3 and 5, respectively in Appendix A in the $SU(2) \times U(1)$ gauge for $\mathcal{L} = 100$ fb^{-1}. By comparing Tables IV and VI, one can confirm that the polarization choices $(\pm 0.8, 0)$ and $(\pm 0.8, \mp 0.3)$ are indeed equivalent to the choices $(\pm 0.4, \mp 0.4)$ and $(\pm 0.6, \mp 0.6)$, respectively. We also obtain limits on the couplings in the $SU(2) \times U(1)$ gauge for the projected plan of the ILC [99]: polarization (0,0) and $(\pm 0.8, 0)$ at $\mathcal{L} = 4$ ab^{-1}, polarization $(\pm 0.8, \mp 0.3)$ and $(\pm 0.8, \mp 0.6)$ at $\mathcal{L} = 3.2$ ab^{-1} and show them in Table VI. Increasing the luminosity from 100 fb^{-1} to the projected luminosity 3.2/4 ab^{-1} the limits on the couplings do not increase proportionately to the luminosity due to the systematic error considered here. If the systematic error is improved, we expect better limits on the couplings; e.g., with no systematic error, the limits can be further improved by a factor of 4 at the projected luminosity.

IV. CONCLUSION

In conclusion, we studied anomalous triple gauge boson couplings in $e^+e^- \to W^+W^-$ with longitudinally polarized beams using W boson polarization observables together with the total cross section and the forward-backward asymmetry for $\sqrt{s} = 500$ GeV and luminosity of $\mathcal{L} = 100$ fb^{-1}. We have 14 anomalous couplings, whereas we have only 10 observables to measure them. So we binned all the observables (A_{fb} excluded) in eight regions of the $\cos\theta_{W^-}$ to increase the number of observables to measure the couplings. We estimated the simultaneous limit on all the couplings for several chosen sets of beam polarization in both the effective vertex formalism and effective operator approach. The limits on the couplings are tighter when $SU(2) \times U(1)$ symmetry is assumed. We show the consistency between the best choice of beam polarizations and minimum likelihood averaged over the anomalous couplings. We find that polarization $(\pm 0.8, \mp 0.6)$ is the best to provide the tightest constraint on the anomalous couplings at the ILC within the technological reach for both 100 fb^{-1} and 3.2 ab^{-1} of luminosity. Our one-parameter limits with unpolarized beams and simultaneous limits for the best polarization choice at 100 fb^{-1} are already much better than the one-parameter limits from experiments; see Table IV. Our analysis considers certain simplifying assumptions, such as the absence of initial-state/final-state radiation and detector effects. While the former might dilute the limits by a small amount, the latter is expected to have no effects on the results as only the leptonic channel is assumed and no flavor tagging or reconstruction is required.

ACKNOWLEDGMENTS

The authors thank Professor Kaoru Hagiwara for useful discussions. R. R. thanks the Department of Science and Technology, Government of India for support through the DST-INSPIRE Fellowship for doctoral program, INSPIRE CODE IF140075, 2014. R. K. S. acknowledges SERB, DST, Government of India through the Project No. EMR/2017/002778.

APPENDIX A: THE DEPENDENCES OF OBSERVABLES ON THE ANOMALOUS COUPLINGS $c_i^{\mathcal{L}}$ AND LIMITS ON THE COUPLINGS $c_i^{\mathcal{O}}/c_i^{\mathcal{L}_g}$ TO THE PROJECTED PLAN OF THE ILC

The anomalous gauge boson couplings $c_i^{\mathcal{O}}$ of the effective operator in Eq. (2), the couplings $c_i^{\mathcal{L}}$ of the Lagrangian in Eq. (4), and the couplings $c_i^{\mathcal{L}_g}$ of the Lagrangian in the $SU(2) \times U(1)$ gauge [given in Eq. (5)] are labeled as

$$c_i^{\mathcal{O}} = \{c_{WWW}, c_W, c_B, c_{\widetilde{WWW}}, c_{\tilde{W}}\}, \tag{A1}$$

TABLE V. The dependence of observables (numerators) on the anomalous couplings in the form of $c_i^{\mathcal{L}}$ (linear), $(c_i^{\mathcal{L}})^2$ (quadratic), and $c_i^{\mathcal{L}} c_j^{\mathcal{L}}, i \neq j$ (interference) in the process $e^+e^- \to W^+W^-$. Here, $V \in \{\gamma, Z\}$. The "✓" (check mark) represents the presence and "⋯" (center dots) corresponds to absence.

Parameters	σ	$\sigma \times A_x$	$\sigma \times A_y$	$\sigma \times A_z$	$\sigma \times A_{xy}$	$\sigma \times A_{xz}$	$\sigma \times A_{yz}$	$\sigma \times A_{x^2-y^2}$	$\sigma \times A_{zz}$	$\sigma \times A_{fb}$
Δg_1^V	✓	✓	⋯	✓	⋯	✓	⋯	✓	✓	✓
g_4^V	⋯	⋯	✓	⋯	✓	⋯	✓	⋯	⋯	⋯
g_5^V	✓	✓	⋯	✓	⋯	✓	⋯	✓	✓	✓
λ^V	✓	✓	⋯	✓	⋯	✓	⋯	✓	✓	✓
$\widetilde{\lambda^V}$	⋯	⋯	✓	⋯	✓	⋯	✓	⋯	⋯	⋯
$\Delta\kappa^V$	✓	✓	⋯	✓	⋯	✓	⋯	✓	✓	✓
$\widetilde{\kappa^V}$	⋯	⋯	✓	⋯	✓	⋯	✓	⋯	⋯	⋯
$(\Delta g_1^V)^2$	✓	✓	⋯	⋯	⋯	⋯	⋯	✓	✓	⋯
$(g_4^V)^2$	✓	⋯	⋯	⋯	⋯	⋯	⋯	✓	✓	⋯
$(g_5^V)^2$	✓	⋯	⋯	⋯	⋯	⋯	⋯	✓	✓	⋯
$(\lambda^V)^2$	✓	✓	⋯	⋯	⋯	⋯	⋯	✓	✓	⋯
$(\widetilde{\lambda^V})^2$	✓	✓	⋯	⋯	⋯	⋯	⋯	✓	✓	⋯
$(\Delta\kappa^V)^2$	✓	✓	⋯	⋯	⋯	⋯	⋯	✓	✓	⋯
$(\widetilde{\kappa^V})^2$	✓	✓	⋯	⋯	⋯	⋯	⋯	✓	✓	⋯
$\Delta g_1^V g_4^V$	⋯	⋯	⋯	⋯	⋯	⋯	✓	⋯	⋯	⋯
$\Delta g_1^V g_5^V$	⋯	⋯	⋯	✓	⋯	⋯	⋯	⋯	⋯	✓
$\Delta g_1^V \lambda^V$	✓	✓	⋯	⋯	⋯	⋯	⋯	✓	✓	⋯
$\Delta g_1^V \widetilde{\lambda^V}$	⋯	⋯	✓	⋯	✓	⋯	⋯	⋯	⋯	⋯
$\Delta g_1^V \Delta\kappa^V$	✓	✓	⋯	⋯	⋯	⋯	⋯	✓	✓	⋯
$\Delta g_1^V \widetilde{\kappa^V}$	⋯	⋯	✓	⋯	✓	⋯	⋯	⋯	⋯	⋯
$g_4^V g_5^V$	⋯	⋯	⋯	⋯	✓	⋯	⋯	⋯	⋯	⋯
$g_4^V \lambda^V$	⋯	⋯	⋯	⋯	⋯	⋯	✓	⋯	⋯	⋯
$g_4^V \widetilde{\lambda^V}$	⋯	⋯	⋯	✓	⋯	✓	⋯	⋯	⋯	✓
$g_4^V \Delta\kappa^V$	⋯	⋯	⋯	⋯	⋯	⋯	✓	⋯	⋯	⋯
$g_4^V \widetilde{\kappa^V}$	⋯	⋯	⋯	✓	⋯	✓	⋯	⋯	⋯	✓
$g_5^V \lambda^V$	⋯	⋯	⋯	✓	⋯	✓	⋯	⋯	⋯	✓
$g_5^V \widetilde{\lambda^V}$	⋯	⋯	⋯	⋯	⋯	⋯	✓	⋯	⋯	⋯
$g_5^V \Delta\kappa^V$	⋯	⋯	⋯	✓	⋯	✓	⋯	⋯	⋯	✓
$g_5^V \widetilde{\kappa^V}$	⋯	⋯	⋯	⋯	⋯	⋯	✓	⋯	⋯	⋯
$\lambda^V \widetilde{\lambda^V}$	⋯	⋯	✓	⋯	✓	⋯	⋯	⋯	⋯	⋯
$\lambda^V \Delta\kappa^V$	✓	✓	⋯	⋯	⋯	⋯	⋯	✓	✓	⋯
$\lambda^V \widetilde{\kappa^V}$	⋯	⋯	✓	⋯	✓	⋯	⋯	⋯	⋯	⋯
$\widetilde{\lambda^V} \Delta\kappa^V$	⋯	⋯	✓	⋯	✓	⋯	⋯	⋯	⋯	⋯
$\widetilde{\lambda^V} \widetilde{\kappa^V}$	✓	✓	⋯	⋯	⋯	⋯	⋯	✓	✓	⋯
$\Delta\kappa^V \widetilde{\kappa^V}$	⋯	⋯	✓	⋯	✓	⋯	⋯	⋯	⋯	⋯

$$c_i^{\mathcal{L}} = \{\Delta g_1^V, g_4^V, g_5^V, \lambda^V, \widetilde{\lambda^V}, \Delta\kappa^V, \widetilde{\kappa^V}\}, \qquad V = \gamma, Z, \quad \text{(A2)}$$

$$c_i^{\mathcal{L}_g} = \{\lambda^V, \widetilde{\lambda^V}, \Delta\kappa^\gamma, \widetilde{\kappa^\gamma}, \Delta g_1^Z, \Delta\kappa^Z, \widetilde{\kappa^Z}\}. \quad \text{(A3)}$$

The dependences of the observables on the anomalous couplings $c_i^{\mathcal{L}}$ are given in Table V. The limits on the couplings $c_i^{\mathcal{O}}$ and $c_i^{\mathcal{L}_g}$ to the projected plan of the ILC are given in Table VI.

TABLE VI. The list of posterior 95% BCI of anomalous couplings $c_i^{\mathcal{O}}$ (TeV^{-2}) of effective operators in Eq. (2) and their translated limits on the couplings $c_i^{\mathcal{L}_g}$ (10^{-2}) for $\sqrt{s} = 500$ GeV and set of luminosities and beam polarizations (ILC projected) in the Binned case from the MCMC with the same notation used in Table III.

(η_3, ξ_3)	(0.0, 0.0)	$(\pm 0.8, 0)$		$(\pm 0.8, \mp 0.3)$		$(\pm 0.8, \mp 0.6)$
$\mathcal{L}$	4 ab^{-1}	100 fb^{-1}	4 ab^{-1}	100 fb^{-1}	3.2 ab^{-1}	3.2 ab^{-1}
$\frac{c_{WWW}}{\Lambda^2}$	$^{+0.44}_{-0.52}$	$^{+1.2}_{-1.1}$	$^{+0.41}_{-0.41}$	$^{+1.1}_{-1.0}$	$^{+0.42}_{-0.41}$	$^{+0.42}_{-0.41}$
$\frac{c_W}{\Lambda^2}$	$^{+0.59}_{-0.50}$	$^{+0.70}_{-0.85}$	$^{+0.27}_{-0.29}$	$^{+0.59}_{-0.75}$	$^{+0.26}_{-0.28}$	$^{+0.25}_{-0.27}$
$\frac{c_B}{\Lambda^2}$	$^{+0.81}_{-1.1}$	$^{+0.81}_{-1.1}$	$^{+0.23}_{-0.25}$	$^{+0.64}_{-0.77}$	$^{+0.19}_{-0.20}$	$^{+0.16}_{-0.17}$
$\frac{c\widetilde{}_{WWW}}{\Lambda^2}$	$^{+0.35}_{-0.35}$	$^{+1.1}_{-1.0}$	$^{+0.37}_{-0.37}$	$^{+0.96}_{-0.97}$	$^{+0.38}_{-0.38}$	$^{+0.38}_{-0.37}$
$\frac{c_{\widetilde{W}}}{\Lambda^2}$	$^{+3.9}_{-3.8}$	$^{+5.9}_{-5.7}$	$^{+1.3}_{-1.3}$	$^{+4.3}_{-4.2}$	$^{+0.97}_{-0.97}$	$^{+0.69}_{-0.69}$
λ^γ	$^{+0.18}_{-0.21}$	$^{+0.51}_{-0.47}$	$^{+0.17}_{-0.17}$	$^{+0.47}_{-0.42}$	$^{+0.18}_{-0.17}$	$^{+0.17}_{-0.17}$
$\widetilde{\lambda^\gamma}$	$^{+0.14}_{-0.15}$	$^{+0.43}_{-0.43}$	$^{+0.15}_{-0.15}$	$^{+0.40}_{-0.40}$	$^{+0.16}_{-0.16}$	$^{+0.16}_{-0.16}$
$\Delta\kappa^\gamma$	$^{+0.15}_{-0.21}$	$^{+0.27}_{-0.38}$	$^{+0.11}_{-0.11}$	$^{+0.24}_{-0.33}$	$^{+0.11}_{-0.12}$	$^{+0.10}_{-0.11}$
$\widetilde{\kappa^\gamma}$	$^{+1.3}_{-1.2}$	$^{+1.9}_{-1.9}$	$^{+0.42}_{-0.42}$	$^{+1.4}_{-1.4}$	$^{+0.31}_{-0.31}$	$^{+0.22}_{-0.22}$
Δg_1^Z	$^{+0.25}_{-0.21}$	$^{+0.29}_{-0.35}$	$^{+0.11}_{-0.12}$	$^{+0.25}_{-0.31}$	$^{+0.11}_{-0.12}$	$^{+0.10}_{-0.11}$
$\Delta\kappa^Z$	$^{+0.29}_{-0.23}$	$^{+0.28}_{-0.30}$	$^{+0.10}_{-0.10}$	$^{+0.22}_{-0.25}$	$^{+0.087}_{-0.092}$	$^{+0.080}_{-0.085}$
$\widetilde{\kappa^Z}$	$^{+0.35}_{-0.36}$	$^{+0.54}_{-0.55}$	$^{+0.12}_{-0.12}$	$^{+0.39}_{-0.39}$	$^{+0.090}_{-0.089}$	$^{+0.064}_{-0.064}$

APPENDIX B: NOTE ON LINEAR APPROXIMATION

If the cross section σ is express as a function of couplings c_i as

$$\sigma = \sigma_0 + \sum_i \sigma_i \times c_i + \sum_{i.j} \sigma_{ij} \times c_i c_j, \tag{B1}$$

linear approximation for the BSM operator will be possible if the quadratic contributions are much smaller than the linear contribution, i.e.,

$$|\sigma_i \times c_i| \gg |\sigma_{ii} \times c_i^2|, \quad \text{or} \quad |c_i| \ll \frac{\sigma_i}{\sigma_{ii}}. \tag{B2}$$

As an example, consider the λ^Z dependent unpolarized cross section given by

$$\sigma(0.0, 0.0) = 1037. + 57. \times \lambda^Z + 12241. \times (\lambda^Z)^{2.} \tag{B3}$$

The linear approximation is valid for $|\lambda^Z| \ll 0.004$. However, the limit on λ^Z is ± 0.36 at 1σ level at 100 fb^{-1} (2% systematic is used) assuming a linear approximation of Eq. (B3), which is much beyond the validity of the linear approximation. To derive a sensible limit one needs to include the quadratic term which appears at $\mathcal{O}(\Lambda^{-4})$. However, at $\mathcal{O}(\Lambda^{-4})$ one also has the contribution from dimension-8 operators at linear order. Our present analysis includes quadratic contributions in dimension-6 operators and does not include dimension-8 contributions to compare our result with the current LHC constrain, Table I. However, at higher luminosity (4 ab^{-1}) we obtain limits on λ^Z to be 10^{-3} using binned observables; see Table VI. In this range of couplings, the linear terms dominate over the quadratic terms and, hence, linear approximation becomes valid. At high luminosity, thus, our analysis effectively considers only $\mathcal{O}(\Lambda^{-2})$-terms in the observables.

APPENDIX C: COMBINING BEAM POLARIZATION WITH ITS OPPOSITE VALUES

To reduce the systematic errors in analysis due to luminosity, the beam polarizations are flipped between two opposite choices frequently giving half the total luminosity to both the polarization choices in an e^+–e^- collider. One can, in principle, use the observables, e.g., the total cross section (σ_T) or their difference (σ_A) as in Eqs. (7) and (8), respectively, or for the two opposite polarization choices (σ & $\bar{\sigma}$) separately for a suitable analysis. In this work, we have combined the opposite beam polarization at the level of χ^2 as given in Eq. (19) not at the level of observables as the former constrains the couplings better than any combinations and of-course the individuals. To depict this, we present the $\chi^2 = 4$ contours of the unbinned cross sections in Fig. 13 (left panel) for beam polarization $(+0.6, -0.6)$ (σ) and $(-0.6, +0.6)$ $(\bar{\sigma})$ and the combinations σ_T and σ_A along with the combined χ^2 in the λ^γ-λ^Z plane for $\mathcal{L} = 50$ fb^{-1} luminosity to each polarization choice as representative. A systematic error of 2% is used as a benchmark in the cross section. The nature of the contours can be explained as follows: In the WW production, the aTGC contributions appear only in the s channel (see Fig. 1), where initial state e^+e^- couples through the

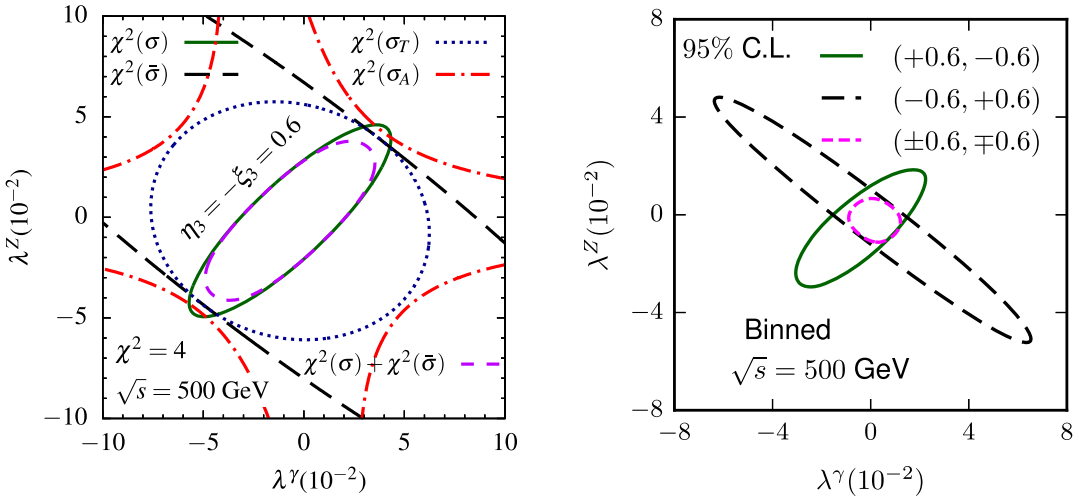

FIG. 13. The $\chi^2 = 4$ contours of the unbinned cross section $\sigma = \sigma(+\eta_3, +\xi_3)$ in solid-green lines, $\bar{\sigma} = \sigma(-\eta_3, -\xi_3)$ in long-dashed-black lines, $\sigma_T = \sigma(+\eta_3, +\xi_3) + \sigma(-\eta_3, -\xi_3)$ in the dotted-blue line, $\sigma_A = \sigma(+\eta_3, +\xi_3) - \sigma(-\eta_3, -\xi_3)$ in the dash-dotted-red line, and the combined χ^2 of σ and $\bar{\sigma}$ in dashed-magenta lines for polarization $(\eta_3, \xi_3) = (+0.6, -0.6)$ on λ^γ-λ^Z plane are shown in the left panel. The 95% C.L. contours from simultaneous analysis in λ^γ-λ^Z plane for the beam polarization $(+0.6, -0.6)$, $(-0.6, +0.6)$ and their combined one $(\pm 0.6, \mp 0.6)$ are shown in the right panel using all the binned observables, i.e., in the Binned case. The analyses are done for $\sqrt{s} = 500$ GeV and $\mathcal{L} = 50$ fb^{-1} luminosity to each beam polarization set.

γ/Z boson and both left and right chiral electrons contribute almost equally. The t-channel diagram, however, is pure background and receives contributions only from left chiral electrons. As a result, the $\bar{\sigma}$ (long-dashed-black) contains more background than σ (solid-green) leading to a weaker limit on the couplings. Further, inclusion of $\bar{\sigma}$ into σ_T (dotted-blue) and σ_A (dashed-dotted-red) reduces the signal to the background ratio, and hence they are less sensitive to the couplings. The total χ^2 for the combined beam polarizations shown in dashed (magenta) is, of course, the best to constrain the couplings. This behavior is reverified with the simultaneous analysis using the binned cross section and polarization asymmetries (72 observables in the Binned case) and shown in Fig. 13 (right panel) in the same λ^γ-λ^Z plane showing the 95% C.L. contours for beam polarizations $(+0.6, -0.6)$, $(-0.6, +0.6)$, and their combinations $(\pm 0.6, \mp 0.6)$. Thus, we choose to combine the opposite beam polarization choices at the level of χ^2 rather than combining them at the level of observables.

[1] S. Chatrchyan *et al.* (CMS Collaboration), Observation of a new boson at a mass of 125 GeV with the CMS experiment at the LHC, Phys. Lett. B **716**, 30 (2012).

[2] C. Bourrely, J. Soffer, and E. Leader, Polarization phenomena in hadronic reactions, Phys. Rep. **59**, 95 (1980).

[3] G. Abbiendi *et al.* (OPAL Collaboration), Measurement of W boson polarizations and CP violating triple gauge couplings from W^+W^- production at LEP, Eur. Phys. J. C **19**, 229 (2001).

[4] I. Ots, H. Uibo, H. Liivat, R. Saar, and R. K. Loide, Possible anomalous Z Z gamma and Z gamma gamma couplings and Z boson spin orientation in $e^+e^- \to Z\gamma$, Nucl. Phys. **B702**, 346 (2004).

[5] F. Boudjema and R. K. Singh, A model independent spin analysis of fundamental particles using azimuthal asymmetries, J. High Energy Phys. 07 (2009) 028.

[6] J. A. Aguilar-Saavedra and J. Bernabeu, Breaking down the entire W boson spin observables from its decay, Phys. Rev. D **93**, 011301 (2016).

[7] R. Rahaman and R. K. Singh, On polarization parameters of spin-1 particles and anomalous couplings in $e^+e^- \to ZZ/Z\gamma$, Eur. Phys. J. C **76**, 539 (2016).

[8] J. Nakamura, Polarisations of the Z and W bosons in the processes $pp \to ZH$ and $pp \to W^\pm H$, J. High Energy Phys. 08 (2017) 008.

[9] W. Buchmuller and D. Wyler, Effective Lagrangian analysis of new interactions and flavor conservation, Nucl. Phys. **B268**, 621 (1986).

[10] K. Hagiwara, S. Ishihara, R. Szalapski, and D. Zeppenfeld, Low-energy effects of new interactions in the electroweak boson sector, Phys. Rev. D **48**, 2182 (1993).

[11] C. Degrande, N. Greiner, W. Kilian, O. Mattelaer, H. Mebane, T. Stelzer, S. Willenbrock, and C. Zhang,

Effective field theory: A modern approach to anomalous couplings, Ann. Phys. (Amsterdam) **335**, 21 (2013).
[12] Z. Zhang, Time to Go Beyond Triple-Gauge-Boson-Coupling Interpretation of W Pair Production, Phys. Rev. Lett. **118**, 011803 (2017).
[13] J. Baglio, S. Dawson, and S. Homiller, QCD corrections in SMEFT fits to WZ and WW production, Phys. Rev. D **100**, 113010 (2019).
[14] K. Hagiwara, R. D. Peccei, D. Zeppenfeld, and K. Hikasa, Probing the weak boson sector in $e^+e^- \to W^+W^-$, Nucl. Phys. **B282**, 253 (1987).
[15] J. Wudka, Electroweak effective Lagrangians, Int. J. Mod. Phys. A **09**, 2301 (1994).
[16] K. J. F. Gaemers and G. J. Gounaris, Polarization amplitudes for $e^+e^- \to W^+W^-$ and $e^+e^- \to ZZ$, Z. Phys. C **1**, 259 (1979).
[17] C. L. Bilchak and J. D. Stroughair, W^+W^- pair production in e^+e^- colliders, Phys. Rev. D **30**, 1881 (1984).
[18] K. Hagiwara, S. Ishihara, R. Szalapski, and D. Zeppenfeld, Low-energy constraints on electroweak three gauge boson couplings, Phys. Lett. B **283**, 353 (1992).
[19] D. Choudhury and J. Kalinowski, Unraveling the $WW\gamma$ and WWZ vertices at the linear collider: Anti-neutrino neutrino γ and anti-neutrino neutrino $\bar{q}q$ final states, Nucl. Phys. **B491**, 129 (1997).
[20] D. Choudhury, J. Kalinowski, and A. Kulesza, CP violating anomalous $WW\gamma$ couplings in e^+e^- collisions, Phys. Lett. B **457**, 193 (1999).
[21] J. D. Wells and Z. Zhang, Status and prospects of precision analyses with $e^+e^- \to W^+W^-$, Phys. Rev. D **93**, 034001 (2016).
[22] G. Buchalla, O. Cata, R. Rahn, and M. Schlaffer, Effective field theory analysis of new physics in $e^+e^- \to W^+W^-$ at a linear collider, Eur. Phys. J. C **73**, 2589 (2013).
[23] L. Berthier, M. Bjørn, and M. Trott, Incorporating doubly resonant $W^\pm$ data in a global fit of SMEFT parameters to lift flat directions, J. High Energy Phys. 09 (2016) 157.
[24] L. Bian, J. Shu, and Y. Zhang, Prospects for triple gauge coupling measurements at future lepton colliders and the 14 TeV LHC, J. High Energy Phys. 09 (2015) 206.
[25] L. Bian, J. Shu, and Y. Zhang, Triple gauge couplings at future hadron and lepton colliders, Int. J. Mod. Phys. A **31**, 1644008 (2016).
[26] S. S. Biswal, M. Patra, and S. Raychaudhuri, Anomalous triple gauge vertices at the large hadron-electron collider, arXiv:1405.6056.
[27] I. T. Cakir, O. Cakir, A. Senol, and A. T. Tasci, Search for anomalous $WW\gamma$ and WWZ couplings with polarized e-beam at the LHeC, Acta Phys. Pol. B **45**, 1947 (2014).
[28] R. Li, X.-M. Shen, K. Wang, T. Xu, L. Zhang, and G. Zhu, Probing anomalous $WW\gamma$ triple gauge bosons coupling at the LHeC, Phys. Rev. D **97**, 075043 (2018).
[29] S. Kumar and P. Poulose, Probing $WW\gamma$ coupling through $e^-\gamma \to \nu_e W^-$ at ILC, Int. J. Mod. Phys. A **30**, 1550215 (2015).
[30] U. Baur and D. Zeppenfeld, Unitarity constraints on the electroweak three vector boson vertices, Phys. Lett. B **201**, 383 (1988).
[31] L. J. Dixon, Z. Kunszt, and A. Signer, Vector boson pair production in hadronic collisions at order α_s: Lepton correlations and anomalous couplings, Phys. Rev. D **60**, 114037 (1999).
[32] A. Falkowski, M. Gonzalez-Alonso, A. Greljo, D. Marzocca, and M. Son, Anomalous triple gauge couplings in the effective field theory approach at the LHC, J. High Energy Phys. 02 (2017) 115.
[33] A. Butter, O. J. P. Éboli, J. Gonzalez-Fraile, M. C. Gonzalez-Garcia, T. Plehn, and M. Rauch, The gauge-higgs legacy of the LHC Run I, J. High Energy Phys. 07 (2016) 152.
[34] A. Azatov, J. Elias-Miro, Y. Reyimuaji, and E. Venturini, Novel measurements of anomalous triple gauge couplings for the LHC, J. High Energy Phys. 10 (2017) 027.
[35] J. Baglio, S. Dawson, and I. M. Lewis, An NLO QCD effective field theory analysis of W^+W^- production at the LHC including fermionic operators, Phys. Rev. D **96**, 073003 (2017).
[36] H. T. Li and G. Valencia, CP violating anomalous couplings in W jet production at the LHC, Phys. Rev. D **96**, 075014 (2017).
[37] J. Baglio, S. Dawson, and I. M. Lewis, NLO effects in EFT fits to W^+W^- production at the LHC, Phys. Rev. D **99**, 035029 (2019).
[38] D. Bhatia, U. Maitra, and S. Raychaudhuri, Pinning down anomalous $WW\gamma$ couplings at the LHC, Phys. Rev. D **99**, 095017 (2019).
[39] M. Chiesa, A. Denner, and J.-N. Lang, Anomalous triple-gauge-boson interactions in vector-boson pair production with RECOLA2, Eur. Phys. J. C **78**, 467 (2018).
[40] R. Rahaman and R. K. Singh, Unravelling the anomalous gauge boson couplings in $ZW^\pm$ production at the LHC and the role of spin-1 polarizations, arXiv:1911.03111.
[41] A. Azatov, D. Barducci, and E. Venturini, Precision diboson measurements at hadron colliders, J. High Energy Phys. 04 (2019) 075.
[42] G. Abbiendi *et al.* (OPAL Collaboration), Measurement of charged current triple gauge boson couplings using W pairs at LEP, Eur. Phys. J. C **33**, 463 (2004).
[43] J. Abdallah *et al.* (DELPHI Collaboration), Study of W boson polarisations and Triple Gauge boson Couplings in the reaction $e^+e^- \to W^+W^-$ at LEP 2, Eur. Phys. J. C **54**, 345 (2008).
[44] S. Schael *et al.* (DELPHI, OPAL, LEP Electroweak, ALEPH, L3 Collaborations), Electroweak measurements in electron-positron collisions at W-boson-pair energies at LEP, Phys. Rep. **532**, 119 (2013).
[45] T. Aaltonen *et al.* (CDF Collaboration), Limits on anomalous triple gauge couplings in $p\bar{p}$ collisions at $\sqrt{s} = 1.96$ TeV, Phys. Rev. D **76**, 111103 (2007).
[46] V. M. Abazov *et al.* (D0 Collaboration), Limits on anomalous trilinear gauge boson couplings from WW, WZ and $W\gamma$ production in $p\bar{p}$ collisions at $\sqrt{s} = 1.96$ TeV, Phys. Lett. B **718**, 451 (2012).
[47] V. Khachatryan *et al.* (CMS Collaboration), Measurement of the WZ production cross section in pp collisions at $\sqrt{s} = 7$ and 8 TeV and search for anomalous triple gauge couplings at $\sqrt{s} = 8$ TeV, Eur. Phys. J. C **77**, 236 (2017).
[48] G. Aad *et al.* (ATLAS Collaboration), Measurements of $W^\pm Z$ production cross sections in pp collisions at

$\sqrt{s} = 8$ TeV with the ATLAS detector and limits on anomalous gauge boson self-couplings, Phys. Rev. D **93**, 092004 (2016).

[49] G. Aad *et al.* (ATLAS Collaboration), Measurement of total and differential W^+W^- production cross sections in proton-proton collisions at $\sqrt{s} = 8$ TeV with the ATLAS detector and limits on anomalous triple-gauge-boson couplings, J. High Energy Phys. 09 (2016) 029.

[50] S. Chatrchyan *et al.* (CMS Collaboration), Measurement of the W^+W^- Cross section in pp Collisions at $\sqrt{s} = 7$ TeV and Limits on Anomalous $WW\gamma$ and WWZ couplings, Eur. Phys. J. C **73**, 2610 (2013).

[51] P. Rebello Teles (CMS Collaboration), Search for anomalous gauge couplings in semi-leptonic decays of $WW\gamma$ and $WZ\gamma$ in pp collisions at $\sqrt{s} = 8$ TeV, in *Meeting of the APS Division of Particles and Fields (DPF 2013) Santa Cruz, California, USA, 2013*, arXiv:1310.0473.

[52] G. Aad *et al.* (ATLAS Collaboration), Measurement of W^+W^- production in pp collisions at $\sqrt{s} = 7$ TeV with the ATLAS detector and limits on anomalous WWZ and $WW\gamma$ couplings, Phys. Rev. D **87**, 112001 (2013); Erratum, Phys. Rev. D **88**, 079906 (2013).

[53] S. Chatrchyan *et al.* (CMS Collaboration), Measurement of the sum of WW and WZ production with $W +$ dijet events in pp collisions at $\sqrt{s} = 7$ TeV, Eur. Phys. J. C **73**, 2283 (2013).

[54] G. Aad *et al.* (ATLAS Collaboration), Measurements of $W\gamma$ and $Z\gamma$ production in pp collisions at $\sqrt{s} = 7$ TeV with the ATLAS detector at the LHC, Phys. Rev. D **87**, 112003 (2013); Erratum, Phys. Rev. D **91**, 119901 (2015).

[55] S. Chatrchyan *et al.* (CMS Collaboration), Measurement of the $W\gamma$ and $Z\gamma$ inclusive cross sections in pp collisions at $\sqrt{s} = 7$ TeV and limits on anomalous triple gauge boson couplings, Phys. Rev. D **89**, 092005 (2014).

[56] M. Aaboud *et al.* (ATLAS Collaboration), Measurement of $WW/WZ \to \ell\nu qq'$ production with the hadronically decaying boson reconstructed as one or two jets in pp collisions at $\sqrt{s} = 8$ TeV with ATLAS, and constraints on anomalous gauge couplings, Eur. Phys. J. C **77**, 563 (2017).

[57] A. M. Sirunyan *et al.* (CMS Collaboration), Search for anomalous couplings in boosted $WW/WZ \to \ell\nu q\bar{q}$ production in proton-proton collisions at $\sqrt{s} = 8$ TeV, Phys. Lett. B **772**, 21 (2017).

[58] M. Aaboud *et al.* (ATLAS Collaboration), Measurements of electroweak Wjj production and constraints on anomalous gauge couplings with the ATLAS detector, Eur. Phys. J. C **77**, 474 (2017).

[59] A. M. Sirunyan *et al.* (CMS Collaboration), Electroweak production of two jets in association with a Z boson in proton-proton collisions at $\sqrt{s} = 13$ TeV, Eur. Phys. J. C **78**, 589 (2018).

[60] A. M. Sirunyan *et al.* (CMS Collaboration), Search for anomalous triple gauge couplings in WW and WZ production in lepton + jet events in proton-proton collisions at $\sqrt{s} = 13$ TeV, J. High Energy Phys. 12 (2019) 062.

[61] A. M. Sirunyan *et al.* (CMS Collaboration), Measurement of electroweak production of a W boson in association with two jets in proton-proton collisions at $\sqrt{s} = 13$ TeV, Eur. Phys. J. C **80**, 43 (2020).

[62] A. M. Sirunyan *et al.* (CMS Collaboration), Measurements of the $pp \to WZ$ inclusive and differential production cross section and constraints on charged anomalous triple gauge couplings at $\sqrt{s} = 13$ TeV, J. High Energy Phys. 04 (2019) 122.

[63] T. Corbett, O. J. P. Éboli, J. Gonzalez-Fraile, and M. C. Gonzalez-Garcia, Determining Triple Gauge Boson Couplings from Higgs Data, Phys. Rev. Lett. **111**, 011801 (2013).

[64] G. Aarons *et al.* (ILC Collaboration), International linear collider reference design report Volume 2: Physics at the ILC, arXiv:0709.1893.

[65] H. Baer, T. Barklow, K. Fujii, Y. Gao, A. Hoang, S. Kanemura, J. List, H. E. Logan, A. Nomerotski, M. Perelstein *et al.*, The international linear collider technical design report—Volume 2: Physics, arXiv:1306.6352.

[66] T. Behnke, J. E. Brau, B. Foster, J. Fuster, M. Harrison, J. M. Paterson, M. Peskin, M. Stanitzki, N. Walker, and H. Yamamoto, The international linear collider technical design report—Volume 1: Executive summary, arXiv:1306.6327.

[67] G. Moortgat-Pick *et al.*, The Role of polarized positrons and electrons in revealing fundamental interactions at the linear collider, Phys. Rep. **460**, 131 (2008).

[68] G. Gounaris, J. Layssac, G. Moultaka, and F. M. Renard, Analytic expressions of cross-sections, asymmetries and W density matrices for $e^+e^- \to W^+W^-$ with general three boson couplings, Int. J. Mod. Phys. A **08**, 3285 (1993).

[69] B. Ananthanarayan, M. Patra, and P. Poulose, W physics at the ILC with polarized beams as a probe of the Littlest Higgs Model, J. High Energy Phys. 11 (2009) 058.

[70] B. Ananthanarayan, M. Patra, and P. Poulose, Signals of additional Z boson in $e^+e^- \to W^+W^-$ at the ILC with polarized beams, J. High Energy Phys. 02 (2011) 043.

[71] B. Ananthanarayan, M. Patra, and P. Poulose, Probing strongly interacting W's at the ILC with polarized beams, J. High Energy Phys. 03 (2012) 060.

[72] V. V. Andreev, G. Moortgat-Pick, P. Osland, A. A. Pankov, and N. Paver, Discriminating Z' from Anomalous Trilinear Gauge Coupling Signatures in $e^+e^- \to W^+W^-$ at ILC with Polarized Beams, Eur. Phys. J. C **72**, 2147 (2012).

[73] J. A. Aguilar-Saavedra, J. Bernabéu, V. A. Mitsou, and A. Segarra, The Z boson spin observables as messengers of new physics, Eur. Phys. J. C **77**, 234 (2017).

[74] F. M. Renard, Polarization effects due to dark matter interaction between massive standard particles, arXiv:1802.10313.

[75] F. M. Renard, Z Polarization in $e^+e^- \to t\bar{t}Z$ for testing the top quark mass structure and the presence of final interactions, arXiv:1803.10466.

[76] F. M. Renard, W polarization in e^+e^-, gluon-gluon and $\gamma\gamma \to Wt\bar{b}$ for testing the top quark mass structure and the presence of final interactions, arXiv:1807.00621.

[77] F. M. Renard, Further tests of special interactions of massive particles from the Z polarization rate in $e^+e^- \to Zt\bar{t}$ and in $e^+e^- \to ZW^+W^-$, arXiv:1808.05429.

[78] F. M. Renard, Z polarization in $e^+e^- \to ZWW$ for testing special interactions of massive particles, arXiv:1807.08938.

[79] S. Behera, R. Islam, M. Kumar, P. Poulose, and R. Rahaman, Fingerprinting the Top quark FCNC via anomalous Ztq couplings at the LHeC, Phys. Rev. D **100**, 015006 (2019).
[80] R. Rahaman and R. K. Singh, On the choice of beam polarization in $e^+e^- \to ZZ/Z\gamma$ and anomalous triple gauge-boson couplings, Eur. Phys. J. C **77**, 521 (2017).
[81] R. Rahaman and R. K. Singh, Anomalous triple gauge boson couplings in ZZ production at the LHC and the role of Z boson polarizations, Nucl. Phys. **B948**, 114754 (2019).
[82] M. Aaboud *et al.* (ATLAS Collaboration), Measurement of $W^{\pm}Z$ production cross sections and gauge boson polarisation in pp collisions at $\sqrt{s} = 13$ TeV with the ATLAS detector, Eur. Phys. J. C **79**, 535 (2019).
[83] A. A. Pankov, N. Paver, and A. V. Tsytrinov, Distinguishing new physics scenarios at a linear collider with polarized beams, Phys. Rev. D **73**, 115005 (2006).
[84] P. Osland, A. A. Pankov, and A. V. Tsytrinov, Identification of extra neutral gauge bosons at the International Linear Collider, Eur. Phys. J. C **67**, 191 (2010).
[85] D. Choudhury and S. D. Rindani, Test of CP violating neutral gauge boson vertices in $e^+e^- \to \gamma Z$, Phys. Lett. B **335**, 198 (1994).
[86] H. Czyz, K. Kolodziej, and M. Zralek, Composite Z boson and CP violation in the process $e^+e^- \to Z\gamma$, Z. Phys. C **43**, 97 (1989).
[87] B. Ananthanarayan and S. D. Rindani, CP violation at a linear collider with transverse polarization, Phys. Rev. D **70**, 036005 (2004).
[88] B. Ananthanarayan, S. D. Rindani, R. K. Singh, and A. Bartl, Transverse beam polarization and CP-violating triple-gauge-boson couplings in $e^+e^- \to \gamma Z$, Phys. Lett. B **593**, 95 (2004); Erratum, Phys. Lett. B **608**, 274 (2005).
[89] A. Bartl, H. Fraas, S. Hesselbach, K. Hohenwarter-Sodek, T. Kernreiter, and G. A. Moortgat-Pick, CP-odd observables in neutralino production with transverse $e+$ and $e-$ beam polarization, J. High Energy Phys. 01 (2006) 170.
[90] K. Rao and S. D. Rindani, Probing CP-violating contact interactions in $e^+e^- \to HZ$ with polarized beams, Phys. Lett. B **642**, 85 (2006).
[91] A. Bartl, K. Hohenwarter-Sodek, T. Kernreiter, and O. Kittel, CP asymmetries with longitudinal and transverse beam polarizations in neutralino production and decay into the Z0 boson at the ILC, J. High Energy Phys. 09 (2007) 079.
[92] H. K. Dreiner, O. Kittel, and A. Marold, Normal tau polarisation as a sensitive probe of CP violation in chargino decay, Phys. Rev. D **82**, 116005 (2010).
[93] O. Kittel, G. Moortgat-Pick, K. Rolbiecki, P. Schade, and M. Terwort, Measurement of CP asymmetries in neutralino production at the ILC, Eur. Phys. J. C **72**, 1854 (2012).
[94] B. Ananthanarayan, S. K. Garg, M. Patra, and S. D. Rindani, Isolating CP-violating γ ZZ coupling in $e^+e^- \to \gamma Z$ with transverse beam polarizations, Phys. Rev. D **85**, 034006 (2012).
[95] J. Alwall, R. Frederix, S. Frixione, V. Hirschi, F. Maltoni, O. Mattelaer, H. S. Shao, T. Stelzer, P. Torrielli, and M. Zaro, The automated computation of tree-level and next-to-leading order differential cross sections, and their matching to parton shower simulations, J. High Energy Phys. 07 (2014) 079.
[96] A. Alloul, N. D. Christensen, C. Degrande, C. Duhr, and B. Fuks, FeynRules 2.0—A complete toolbox for tree-level phenomenology, Comput. Phys. Commun. **185**, 2250 (2014).
[97] A. Vauth and J. List, Beam Polarization at the ILC: Physics Case and Realization, Int. J. Mod. Phys. Conf. Ser. **40**, 1660003 (2016).
[98] G. Moortgat-Pick, Physics aspects of polarized e+ at the linear collider, in 1st International Positron Source Workshop (POSIPOL 2006) Geneva, Switzerland, 2006, http://weblib.cern.ch/abstract?CERN-PH-TH-2006-128.
[99] T. Barklow, J. Brau, K. Fujii, J. Gao, J. List, N. Walker, and K. Yokoya, ILC operating scenarios, arXiv:1506.07830.
[100] P. Bambade *et al.*, The international linear collider: A global project, arXiv:1903.01629.